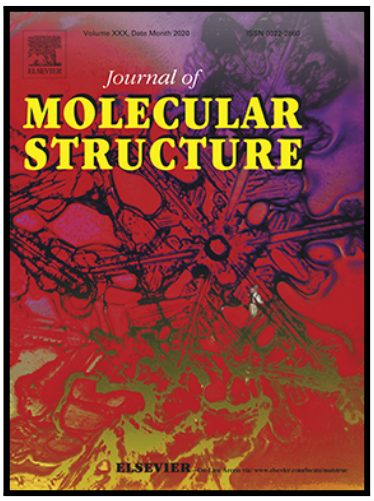

A Simplistic Approach for Preparation of Alkylidenemalononitrile Derivatives: Characterization, In silico Studies, Quantum Chemical Evaluation, Molecular Docking, and In vitro Biological Activity Evaluation

Iqbal Azad , Tahmeena Khan , Rumana Ahmad , Azhar Kamal , Abdul Rahman Khan , Malik Nasibullah

PII: S0022-2860(20)31766-X
DOI: https://doi.org/10.1016/j.molstruc.2020.129451
Reference: MOLSTR 129451

To appear in: *Journal of Molecular Structure*

Received date: 8 May 2020
Revised date: 30 September 2020
Accepted date: 13 October 2020

Please cite this article as: Iqbal Azad , Tahmeena Khan , Rumana Ahmad , Azhar Kamal , Abdul Rahman Khan , Malik Nasibullah , A Simplistic Approach for Preparation of Alkylidenemalononitrile Derivatives: Characterization, In silico Studies, Quantum Chemical Evaluation, Molecular Docking, and In vitro Biological Activity Evaluation, *Journal of Molecular Structure* (2020), doi: https://doi.org/10.1016/j.molstruc.2020.129451

Highlights

- Twelve different malononitrile derivatives *via* Knoevenagel condensation were synthesized
- *In vitro* antibacterial and anticancer activities using the disc diffusion and MTT assay respectively
- Metabolic transformation, molecular parameters, druglikeness, ADMET
- Molecular docking was performed with tyrosine-protein kinase and ribonucleoside-diphosphate reductase

A Simplistic Approach for Preparation of Alkylidenemalononitrile Derivatives: Characterization, *In silico* Studies, Quantum Chemical Evaluation, Molecular Docking, and *In vitro* Biological Activity Evaluation

Iqbal Azad[1*], Tahmeena Khan[1], Rumana Ahmad[2], Azhar Kamal[3], Abdul Rahman Khan[1], Malik Nasibullah[1]

[1]Department of Chemistry, Integral University, Dasauli, P.O. Bas-ha, Kursi Road, Lucknow-226026, U.P., India
[2]Department of Biochemistry, Era's Lucknow Medical College and Hospital, Era University, Lucknow, 226003, U.P., India
[3]Department of Bioengineering, Integral University, Dasauli, P.O. Bas-ha, Kursi Road, Lucknow-226026, U.P., India
*iqbalazad@iul.ac.in

Abstract

A new and efficient green grinding-based catalyst free Knoevenagel condensation of aldehydes/ketones and malononitrile for the rapid preparation of twelve malononitrile derivatives (C1-C12) is proposed. Characterization of the derivatives was done by ^{1}H NMR, ^{13}C NMR, IR, elemental and mass spectral analyses. Quantum chemical calculations were performed by DFT/B3LYP/6-31G(d,p) method. The experimental and theoretical spectra were found to be in good agreement with each other. Natural bond order (NBO) calculations were also performed to calculate the natural atomic charges at atomic sites. The present study also involved study of the intramolecular charge transfer (ICT) interactions and the non-linear optical (NLO) properties. Critical drug character assessment parameters like metabolic transformation, druglikeness, ADMET (absorption, distribution, metabolism and excretion) and toxicological analyses of the synthesized malononitrile derivatives were also performed. Molecular docking studies were performed against two target proteins *viz.* tyrosine-protein kinase (HCK) and ribonucleoside diphosphate reductase (RR). The synthesized malononitrile derivatives were also evaluated for their anticancer activity against the triple negative breast cancer (TNBC) cell line (MDA-MB-231) while their antibacterial potential was tested against *S. aureus* and *E. coli*.

Keywords: Knoevenagel condensation; Grinding; Cancer; Molecular Docking; Nonlinear Optical Activity; NBO calculations

Introduction

Malononitrile derivatives are multipurpose building blocks used for the synthesis of different biological and pharmacological molecules [1–4]. In recent investigations, malononitrile scaffolds have been largely utilized to synthesize novel bioactive motifs such as 2-amino-4-(furan-2-yl)-6-(naphthalen-2-yl)-4,5-dihydropyridine-3-carbonitrile (**3**) and hexahydrospiro[indeno[2,1-c]pyridazine-9,5'-pyrano[2,3-d]pyrimidine]-4,6'-dicarbonitrile derivative (**6**) with significant antibacterial and anticancer potency [5,6].

Many malononitrile derivatives such as (E)-2-(3-(4-aminostyryl)-5,5-dimethylcyclo-hex-2-enylidene)malononitrile, 2-(4-oxo-3-phenylthiazolidin-2-ylidene) malononitrile and (2-dicyanomethylene-4,5,5-trimethyl-2,5-dihydrofur-an-3-carbonitrile) are also well known as organic non-linear optical (NLO) materials, because of their applications in

telecommunications and optical information processes. Nowadays, di-2-(2-oxindolin-3-ylidene)malononitrile (DIM) (**2**), 2-(2,4-dimethoxybenzylidene) malononitrile (DMM) (**1**), (E)-2-(1-(7-(diethylamino)-2-oxo-2H-chromen-3-yl)-3-(4-(diphenylamino)phenyl)allylidene) malononitrile (**4**) and (E)-2-(1-(4-aminophenyl)-3-(4-(diphenylamino) phenyl)allylidene) malononitrile (**5**) derivatives **(Figure 1)** are being developed as air-stable n-type organic field-effect transistors (OFETs), organic semiconductors (OSCs) and NLO crystals material [7–9]. Zych and Slodek (2020) have proposed an efficient synthetic route for the preparation of substituted triazole malononitrile derivatives with high yield (65-85%). The synthesized compounds have been found to display interesting optical, photophysical, biological as well as fluorescence properties [10].

Organic reactions under catalyst-free and solvent-free conditions have received considerable attention particularly in green chemistry [11]. The Knoevenagel condensation is a nucleophilic addition reaction of the carbonyl group (aldehyde/ketone) and active hydrogen compounds for constructing an α, β unsaturated structure followed by elimination of a water molecule [12]. This reaction is catalyzed by aliphatic amines such as ethylenediamine, piperidine and ammonium salts, amino acids like glycine, β-alanine and L-proline etc. and produces better yield in protic solvents such as water, ethanol and N,N-dimethylformamide (DMF) etc. [13]. Microwave irradiation has also shown its utility under solvent-free condition. At room temperature, Knoevenagel condensation reaction has not been achieved between the aromatic carbonyl group and active hydrogen compounds [14]. Demchuk et al. (2011) proposed a simple grinding procedure for the synthesis of (2-oxo-1,2-dihydro-3H-indol-3-ylidene) malononitriles at RT in the presence of 1-5 equivalents of water within 15 min [15].

In the present paper, synthesis of malononitrile derivatives, using the grinding method *via* Knoevenagel condensation reaction and investigation of their anticancer and antibacterial activity has been reported. Density functional theory (DFT) was used to evaluate nonlinear optical activity (NLO), natural bond order (NBO) and reactivity descriptors. Computer-aided studies were also performed for the analysis of druglikeness and toxicity of the synthesized compounds. All the results were compared with standard anticancer and antibiotic drugs *viz.* doxorubicin hydrochloride and tetracycline. The synthesized malononitrile derivatives [16] were docked against two protein targets *viz.* i. tyrosine-protein kinase (HCK; PDB ID: 5ZJ6), whose elevated expression is found in several solid carcinomas including breast cancer [17] which is responsible for aberrant signaling pathways leading to defective cell cycle and uncontrolled cell division and ii. ribonucleotide diphosphate reductase (RR; PDB ID: 6AUI), another important enzyme for providing DNA building blocks crucial for cellular propagation [18].

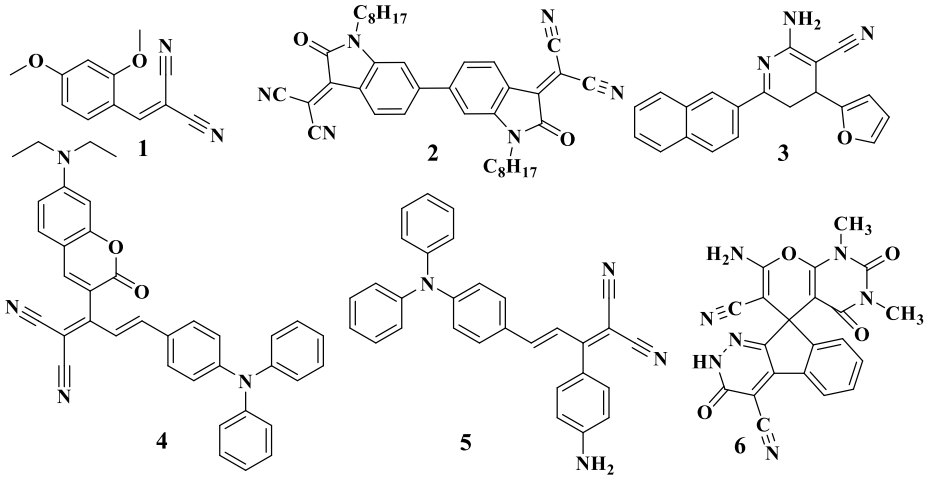

Figure 1. A few examples of recently investigated malononitrile derivatives as n-type organic field-effect transistors (OFETs), organic semiconductors (OSCs), NLO crystals material and biological activate motif.

Experimental and computational methods

Chemistry

Synthesis of 2-benzylidenemalononitrile and of 2-(2-oxo-indolin-3-ylidene) malononitrile derivatives

Malononitrile (66 mg, 1 mmol) and 2,4-dichlorobenzaldehyde (223 mg, 1 mmol) were taken in pestle-mortar and mixed in 1:1 molar ratio in PEG-400/water as a solvent. After 10 min of grinding yellowish solid was obtained which was washed with water/ethanol (2×10 mL) and the reaction was monitored by TLC using hexane and acetyl acetate (8:2) as the eluent and silica gel as stationary phase. TLC plates were visualized in an iodine chamber. After air drying and recrystallization in ethanol for 24 h, a white crystalline solid was obtained with high yield (96-99%) and characterized (Supplementary information) **Scheme 1** and **Table 1**.

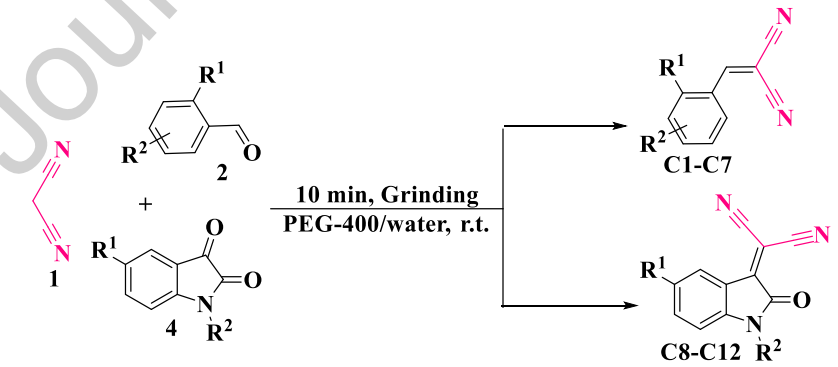

Scheme 1. Synthesis of malononitrile derivatives

Characterization details

1. 2-(2,6-dichlorobenzylidene)malononitrile (C1): White crystalline solid, m.p. 89-91°C, FT-IR (KBr, *v*, cm^{-1}): 3086 (C-H, alkene), 3024 (C-H, ring), 2238 (CN), 1612 (C=C,

aromatic), 1558, 1429, 1145, 772 (Cl), 696. ^{1}H NMR (400 MHz, $CDCl_3$): δ 7.90 (s, 1H, CH=), 7.37 (d, *J = 4.6* Hz, 2H, ArH), 7.21- 7.19 (m, 1H, ArH). ^{13}C NMR ($CDCl_3$): δ 156.7, 134.2, 132.9, 128.9, 111.9, 110.6, 94.3. HRMS (ESI-TOF, m/z) Calcd. for $C_{10}H_4Cl_2N_2$ (M + H^+): 223.01, Found: 222.98. Anal. Calcd. for $C_{10}H_4Cl_2N_2$: C, 53.85; H, 1.81; N, 12.56, Found: C, 53.65; H, 1.67; N, 12.43.

2. 2-(2,4-dichlorobenzylidene)malononitrile (C2): White crystalline solid, m.p. 157-159°C, FT-IR (KBr, *v*, cm^{-1}): 3102 (C-H, alkene), 3050 (C-H, ring), 2227 (CN), 1602 (C=C, aromatic), 1573, 1463, 1367, 823, 793 (Cl), 757. ^{1}H NMR (400 MHz, $CDCl_3$): δ 8.12 (s, 1H, CH=), 7.51 (s, 1H, ArH), 7.38 (d, *J = 1.8* Hz, 1H, ArH), 7.36 (d, *J = 1.8* Hz, 1H, ArH). ^{13}C NMR ($CDCl_3$): δ 154.7, 141.2, 137.3, 130.9, 130.3, 128.5, 127.6, 113.2, 111.9, 86.2. HRMS (ESI-TOF, m/z) Calcd. for $C_{10}H_4Cl_2N_2$ (M + H^+): 223.01, Found: 222.98. Anal. Calcd. for $C_{10}H_4Cl_2N_2$: C, 53.85; H, 1.81; N, 12.56, Found: C, 53.63; H, 1.71; N, 12.46.

3. 2-(furan-2-ylmethylene)malononitrile (C3): Pail yellow crystalline solid, m.p. 74-76°C, FT-IR (KBr, *v*, cm^{-1}): 3124 (C-H, alkene), 3043 (C-H, ring), 2227 (CN), 1603 (C=C, aromatic), 1529, 1463, 1397, 1146, 933, 889, 793, 765. ^{1}H NMR (400 MHz, $CDCl_3$): δ 7.75 (s, 1H), 7.46 (d, *J = 3.1* Hz, 1H, furyl), 7.20 (d, *J = 2.7* Hz, 1H, furyl), 6.66 (t, *J = 5.2* Hz, 1H, furyl). ^{13}C NMR ($CDCl_3$): δ 149.7, 148.1, 143.2, 123.7, 114.6, 113.9, 112.7. HRMS (ESI-TOF, m/z) Calcd. for $C_8H_4N_2$ (M + H^+): 144.98, Found: 145.13. Anal. Calcd. for $C_8H_4N_2$: C, 66.67; H, 2.80; N, 19.44, Found: C, 66.69; H, 2.76; N, 19.44.

4. 2-(4-(dimethylamino)benzylidene)malononitrile (C4): Orange-red crystalline solid, m.p. 187-189°C, FT-IR (KBr, *v*, cm^{-1}): 2935 (C-H, alkene), 2905 (C-H, ring), 2815, 2205 (C≡N), 1610 (C=C, aromatic), 1558, 1352, 926, 816, 727. ^{1}H NMR (400 MHz, $CDCl_3$): δ 7.82 (d, *J = 9.2* Hz, 2H, ArH), 7.47 (s, 1H, CH=), 6.69 (d, *J = 9.3* Hz, 2H, ArH), 3.15 (s, 6H, CH_3). ^{13}C NMR ($CDCl_3$): δ 158.2, 154.4, 133.9, 119.4, 116.1, 115.1, 111.7, 72.0, 40.2. HRMS (ESI-TOF, m/z) Calcd. for $C_{12}H_{11}N_3$ (M + H^+): 198.10, Found: 198.10. Anal. Calcd. for $C_{12}H_{11}N_3$: C, 73.07; H, 5.62; N, 21.30, Found: C, 73.15; H, 5.71; N, 21.38.

5. 2-benzylidenemalononitrile (C5): Yellowish white crystalline solid, m.p. 83-85°C, FT-IR (KBr, *v*, cm^{-1}): 3151 (C-H, alkene), 3028 (C-H, ring), 2227 (C≡N), 1595 (C=C, aromatic), 1441, 963, 793, 757, 676. ^{1}H NMR (400 MHz, $CDCl_3$): δ 8.07 (s, 1H, CH=), 7.32 – 7.17 (m, 5H, ArH). ^{13}C NMR ($CDCl_3$): δ 160.1, 134.7, 131.0, 130.8, 129.7, 113.8, 112.6, 82.83. HRMS (ESI-TOF, m/z) Calcd. for $C_{10}H_6N_2$ (M + H^+): 155.08, Found: 155.05. Anal. Calcd. for $C_{10}H_6N_2$: C, 77.91; H, 3.92; N, 18.17, Found: C, 77.87; H, 3.89; N, 18.21.

6. 2-((1H-indol-3-yl)methylene)malononitrile (C6): Dark yellowish powder, m.p. 178-180°C, FT-IR (KBr, *v*, cm^{-1}): 3271, 3051 (C-H, alkene), 2927 (C-H, ring), 2220 (C≡N), 1624 (C=C, aromatic), 1588, 1565, 1441, 1338, 1235, 1146, 793, 735. ^{1}H NMR (400 MHz, $CDCl_3$): δ 10.00 (s, 1H, NH), 8.27 (s, 1H, CH=) 7.79 (s, 1H, ArH), 7.45 (d, *J = 2.2* Hz, 1H, ArH), 7.37 (d, *J = 1.8* Hz, 1H, ArH), 7.35-7.21 (m, 2H ArH). ^{13}C NMR ($CDCl_3$): δ 150.6, 136.6, 132.2, 126.5, 123.3, 122.0, 121.0, 117.5, 115.4, 112.6, 111.8, 70.2. HRMS (ESI-TOF, m/z) Calcd. for $C_{12}H_7N_3$ (M + H^+): 194.07, Found: 194.06. Anal. Calcd. for $C_{12}H_7N_3$: C, 77.91; H, 3.92; N, 18.17, Found: C, 77.97; H, 3.95; N, 18.22.

7. 2-(4-hydroxy-3-methoxybenzylidene)malononitrile (C7): Reddish-yellow crystalline solid, m.p. 132-134°C, FT-IR (KBr, *v*, cm^{-1}): 3403, 3027, 2981, 2227, 1661, 1617, 1565, 1514, 1455, 1382, 1293, 1176, 1022, 955, 816, 793, 727. ^{1}H NMR (400 MHz, $CDCl_3$): δ 8.03 (s, 1H, CH=), 7.23 (d, *J = 1.8* Hz, 1H, ArH), 7.19 (s, 1H, ArH), 6.95 (d, *J = 8.0* Hz, 1H, ArH), 4.30 (s, 1H, OH), 3.91 (s, 3H, OCH_3). ^{13}C NMR ($CDCl_3$): δ 159.3, 153.7, 147.8, 128.2, 122.8, 115.7, 114.5, 113.7, 111.5, 75.6, 55.5. HRMS (ESI-TOF, m/z) Calcd. for $C_{11}H_8N_2$ (M+ H^+): 201.08, Found: 201.06. Anal. Calcd. for $C_{11}H_8N_2$: C, 66.00; H, 4.03; N, 13.99, Found: C, 65.34; H, 3.87; N, 14.27.

8. 2-(2-oxo-indolin-3-ylidene)malononitrile (C8): Dark red powder, m.p. 240-242°C, FT-IR (KBr, *v*, cm^{-1}): 3256, 3109, 2235, 1712, 1617, 1588, 1338, 793. ^{1}H NMR (400 MHz, DMSO-d_6): δ 11.43 (s, 1H, NH), 8.14 (d, *J = 7.6* Hz, 1H, ArH), 7.57-7.52 (m, 1H, ArH), 7.18-7.14 (m, 1H, ArH), 6.94 (d, *J = 8.2* Hz, 1H, ArH). ^{13}C NMR (DMSO-d_6): δ 163.7, 150.5, 146.4, 137.8, 125.8, 122.9, 118.5, 113.0, 111.6, 111.5, 80.5. HRMS (ESI-TOF, m/z) Calcd. for $C_{11}H_5N_3$ (M^+ H^+): 196.02, Found: 196.04. Anal. Calcd. for $C_{11}H_5N_3$: C, 67.69; H, 2.58; N, 21.53, Found: C 67.49, H 2.71, N 21.54.

9. 2-(2-oxo-1-phenylindolin-3-ylidene)malononitrile (C9): Reddish-black powder, m.p. 195-197°C, FT-IR (KBr, *v*, cm^{-1}): 3095, 2227, 1712, 1610, 1588, 1463, 1367, 1184, 793. ^{1}H NMR (400 MHz, DMSO-d_6): δ 7.78 (d, *J = 4.6* Hz, 1H, ArH), 7.53-7.36 (m, 4H, ArH), 7.21-7.09 (m, 4H, ArH). ^{13}C NMR (DMSO-d_6): δ 162.1, 149.3, 147.2, 137.9, 132.5, 130.1, 129.3, 127.0, 126.3, 124.5, 118.3, 112.5, 111.1, 110.7, 109.1, 83.0. HRMS (ESI-TOF, m/z) Calcd. for $C_{17}H_9N_3$ (M + H^+): 272.13, Found: 272.07. Anal. Calcd. for $C_{17}H_9N_3$: C, 75.27; H, 3.34; N, 15.49, Found: C, 75.19; H, 3.42; N, 15.61.

10. 2-(1-methyl-2-oxoindolin-3-ylidene)malononitrile (C10): Reddish-black powder, m.p. 227-229°C, FT-IR (KBr, *v*, cm^{-1}): 3082, 2919, 2235, 1720, 1611, 1595, 1463, 1331, 1227, 786. ^{1}H NMR (400 MHz, DMSO-d_6): δ 7.85 (d, *J = 6.7* Hz, 1H, ArH), 7.59-7.52 (m, 1H, ArH), 7.39 (d, *J = 6.6* Hz, 1H, ArH), 7.15-7.08 (m, 1H, ArH), 3.39 (s, 3H, CH_3). ^{13}C NMR (DMSO-d_6): δ 181.2, 143.4, 140.6, 129.8, 127.0, 125.9, 123.5, 111.6, 110.6, 92.1, 24.4. HRMS (ESI-TOF, m/z) Calcd. for $C_{12}H_7N_3$ (M + H^+): 210.07, Found: 210.06. Anal. Calcd. for $C_{12}H_7N_3$:C, 68.89; H, 3.37; N, 20.09, Found: C 68.96, H 3.25, N 20.10.

11. 2-(5-bromo-2-oxoindolin-3-ylidene)malononitrile (C11): Reddish-black powder, m.p. 236-238°C, FT-IR (KBr, *v*, cm^{-1}): 3573, 3507, 3097, 2984, 2235, 1727, 1621, 1595, 1463, 1308, 823, 793. ^{1}H NMR (400 MHz, DMSO-d_6): δ 11.33 (s, 1H, NH), 7.93 (s, 1H, ArH), 7.64 (d, *J = 4.5* Hz, 1H, ArH), 6.94 (d, *J = 4.3* Hz, 1H, ArH). ^{13}C NMR (DMSO-d_6): δ 162.6, 144.9, 139.3, 127.9, 119.3, 114.3, 112.8, 111.4, 109.9, 81.7. HRMS (ESI-TOF, m/z) Calcd. for $C_{11}H_4N_3$ (M + H^+): 274.27, Found: 273.95. Anal. Calcd. for $C_{11}H_4N_3$: C, 48.21; H, 1.47; N, 15.33, Found: C 48.11, H 1.53, N 15.47.

12. 2-(2-oxo-acenaphthylen-1(2H)-ylidene)malononitrile (C12): Brown powder, m.p. 260-262°C, FT-IR (KBr, *v*, cm^{-1}): 3086, 2919, 2227, 1720, 1595, 1573, 1485, 1286, 838, 779. ^{1}H NMR (400 MHz, DMSO-d_6): δ 8.19 (d, *J = 6.7* Hz, 1H, ArH), 8.13 (d, *J = 10.8* Hz, 1H, ArH), 7.99 (d, *J = 14.4* Hz, 1H, ArH), 7.79 (d, *J = 13.1* Hz, 1H, ArH), 7.63-7.49 (m, 2H,

ArH). HRMS (ESI-TOF, m/z) Calcd. for $C_{15}H_6N_2$ ($M + H^+$): 231.06, Found: 231.06. Anal. Calcd. for $C_{15}H_6N_2$: C, 78.26; H, 2.63; N, 12.17, Found: C, 78.31; H, 2.52; N, 12.27.

Table 1. Physico-chemical characterization details of compounds (C1-C12) with optimized and MetaPrint2D structures

Entry	Precursor	Product	Rf	Isolate yield (%)	Melting point (°C)	MetaPrint2D Structure
C1	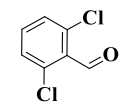	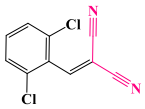	0.67	99	89-91	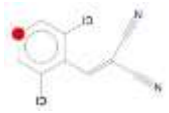
C2	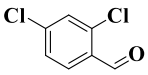	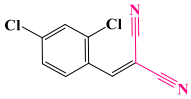	0.76	99	157-159	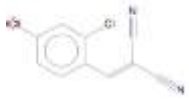
C3	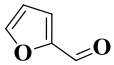	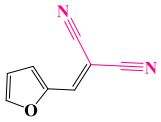	0.44	71	74-76	
C4	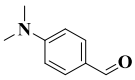	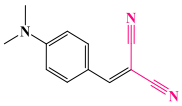	0.31	98	187-189	
C5	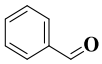	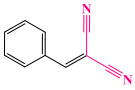	0.70	69	83-85	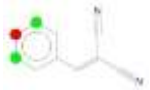
C6	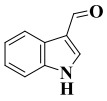	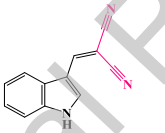	0.22	97	178-180	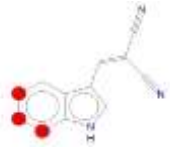
C7	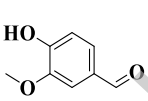	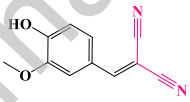	0.25	98	132-134	
C8	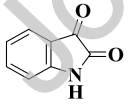	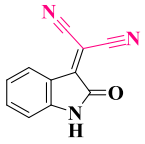	0.15	97	240-242	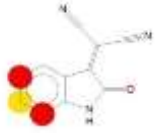
C9	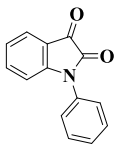	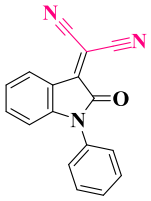	0.35	99	195-197	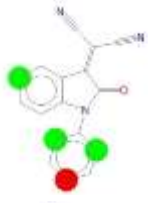
C10	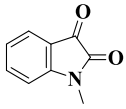		0.19	99	227-229	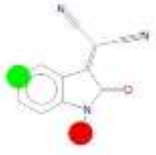

C11	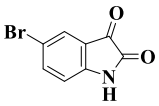	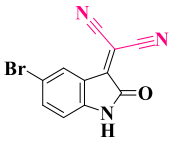	0.18	99	236-238	
C12	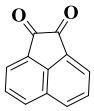	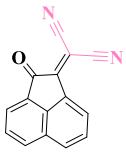	0.32	99	260-262	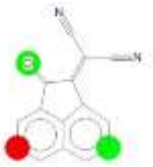

Experimental

Spectral assessment

All the chemicals used were of A.R. grade and purchased from Sigma Aldrich. The melting points of synthesized compounds were determined by open capillary method on digital melting point apparatus (Model 634, Electronics India (EI), Himachal Pradesh, India). Thin layer chromatography (TLC) was performed on silica gel G coated plates using ethyl acetate-hexane (2:8) mixture as eluent and visualization was carried out using iodine vapor. Elemental analysis (C, H and N) was performed on EuroVector elemental analyzer. UV-Visible spectra (200-500 nm) were recorded on ELICO SL-160 double beam spectrophotometer equipped with a 10 mm quartz cell. The IR spectra ν (cm^{-1}) (KBr) were recorded on an Agilent Cary 630 FTIR spectrometer in the frequency range 4000-450 cm^{-1}. The ^{1}H NMR and ^{13}C NMR spectra were obtained on a BrukerAvance400 (NMR) at 400 MHz, using tetramethylsilane (TMS) as an internal reference and $CDCl_3$/DMSO-d_6 as solvent. Mass spectrometry was performed on Agilent 6520 Q-TOF mass spectrometer with electro spray ionization (ESI) probe.

Biological Activity Evaluation

All biological evaluation studies were carried out at Cell and Tissue Culture Lab, Dept. of Biochemistry, Era's Lucknow Medical College, Era University, Lucknow. Human breast carcinoma cell line MDA-MB-231 cell line was maintained by sub-culturing and passaging as monolayers in 25 and 75 cm^2 cell culture flasks (Nest, Tarsons) at 37°C in a 5% CO_2 incubator at 95% humidity for producing H_2CO_3 buffering capacity as reported earlier. The cells were maintained at pH 7.4 in DMEM containing phenol red as a pH indicator and supplemented with 5% FBS [19]. The medium, prior to being used in cell culture experiments was vacuum filtered using a Corning filtration system (Corning®, Sigma-Aldrich).

Anticancer Activity

0.1 M solutions of the compounds were prepared in 1.0 mL 50% DMSO solution. The solutions were diluted 10 times in DMEM to give 0.01 M (10 µM) solutions. In separate experiments, cells were trypsinized and cultured in 6-well (0.5×10^5 cells/well) initially for 24 h, to allow the cells to adhere. After 24 h of incubation, the cells were exposed to 20-100 µM of the synthesized malononitrile derivatives (C1-C12) for the next 48 h. Suitable untreated controls (containing 50% DMSO as a vehicle) were also concomitantly employed. Each dose

was tested in at least 3 replicate wells. For morphological analysis, cells in 6-well plate were observed under phase contrast microscope (Nikon Eclipse Ti, Japan) & photographed.

Methyl tetrazolium-MTT assay

MTT was performed as per published protocol in 96-well microliter tissue culture plates (Linbro, MP Biomedicals) [20]. For MTT assay, 10^4 MDA cells were seeded in 200 µL of the medium in a 96-well microliter tissue culture plate and cultured in a humidified 5% CO_2 incubator at 37°C for 24 h. Defined concentrations (20, 50 and 100 µM) of the compounds in 50% DMSO were freshly prepared in culture media by serial dilution. Serial dilution was carried out in cell culture media in such a way that the final concentration of DMSO in the well did not exceed 0.5% (v/v). Three control wells containing medium alone to serve as blanks were also included. After 24 h of incubation, in separate experiments, cells were treated with the above-mentioned concentrations of the synthesized compounds C1-C12 in triplicates for 48 h. Equal volumes of 50% DMSO (in cell culture media) were used as vehicle controls. At the end of treatment, cell culture medium containing varying amounts of synthesized compounds was removed and 20 µL of MTT (stock made in PSS at 5.0 mg/mL) reagent was added to each well and incubated for 4 h. Thereafter, MTT was removed and formazan crystals were dissolved in 200 µL of DMSO. The plates were read in a Bio-Rad PW41 ELISA plate reader at a wavelength of 570 nm with a reference wavelength of 630 nm. Percentage cell viability (Y-axis) was calculated from absorbance and plotted against concentration in µM (X-axis).

% Cell survival was calculated as = $\left\{\left(A_T - A_B\right) - \left(A_c - A_B\right)\right\} \times 100$ (1)

where,

A_T = Absorbance of treatment well

A_B = Absorbance of blank

A_C = Absorbance of control well

% cell inhibition = 100-Cell Survival

IC_{50} values were obtained from the graph as the concentration which decreased cell by viability 50%.

Antibacterial Activity

The *in vitro* antibacterial activity of the compounds was evaluated against *Staphylococcus aureus* (Gram positive) and *Escherichia coli* (Gram-negative) bacteria by disc diffusion method [21] using Mueller-Hinton agar (MHA) medium. The bacteria were sub-cultured in the agar medium and were incubated for 24 h at 37°C. The discs (Sterile filter paper discs, Whatman No. 1.0) having a diameter of 5 mm, were then soaked in the test solutions with the appropriate equivalent amounts of the synthesized compounds dissolved in sterile 50% DMSO at concentrations of 2-10 mg/disc and placed on lawn culture of the respective microbial organism and stored in an incubator for the above mentioned period of time [22]. Formation of inhibition zone (if any) around each disc was measured and the results recorded in the form of inhibition zones as a function of diameter (mm). To clarify

any effect of DMSO (used as a vehicle for the dissolution of the synthesized compounds) on biological screening, 50% DMSO was used as a negative control where it showed no activity against any bacterial strains. Tetracycline was used as a positive control [21].

Computational details

Density Functional Theory (DFT) calculations

The geometries of the synthesized compounds, were determined and explored using DFT with Becke's three-parameter functional and Lee-Yang-Parr functional hybrid model (B3LYP) combined with 6-31G(d,p) basis set. DFT based calculations were done by Gauss View v6.0 and Gaussian 09W program package [23,24]. The frequency analysis and optimization of the alkylidene malononitrile derivatives were executed at the same level of theory and were scaled by a factor of 0.9679. Potential energy distribution (PED) analysis was performed by VEDA4 program. Optimized geometries were further used for the DFT based global reactivity descriptor analysis including E_{HOMO} (energy of highest occupied molecular orbital), E_{LUMO} (energy of lowest unoccupied molecular orbital energy), E_{GAP} (band gap energy), absolute softness (σ), absolute hardness (η), optical softness (σ_0), chemical potential (CP), absolute electronegativity (χ), additional electronic charges (ΔN_{max}) nucleophilicity index (N) and electrophilicity index (ω) [25]. Molecular electrostatic potential surface (MEP) analysis was also done. Gauge independent atomic orbital (GIAO) method was used to evaluate ^{1}H and ^{13}C NMR spectra. The UV-Vis absorption spectra were calculated using the Time-Dependent Density Functional Theory (TD-DFT) calculations and also used for the calculation of oscillator strengths (OS). Non-linear optical (NLO) parameters such as total static dipole moment (μ), the mean polarizability (α_0), the anisotropy of the polarizability (Δα) and the first hyperpolarizability (β_0) were also calculated and natural bond order (NBO) analysis was done *via* NBO v6.0 program to identify inter and intra-molecular delocalization strength and interaction [26].

In-silico bioactivity analysis

Molecular Docking

The synthesized compounds were subjected to molecular docking using the AutoDock Tools (ADT) v1.5.6 and Auto Dock v4.0.1 (interactive molecular graphics programs) to understand the drug-receptor interaction with the target receptor enzymes. The results were further validated with iGEMDOCK v2.1.

Preparation of the receptor for docking (AutoDock)

The X-ray crystal structures of tyrosine-protein kinase HCK (PDB ID: 5ZJ6, UniProtKB ID: P08631, HCK_HUMAN) and ribonucleoside diphosphate-reductase (PDB ID: 6AUI, UniProtKB ID: P23921, RIR1_HUMAN) were obtained from the Protein Data Bank in PDB format [27].

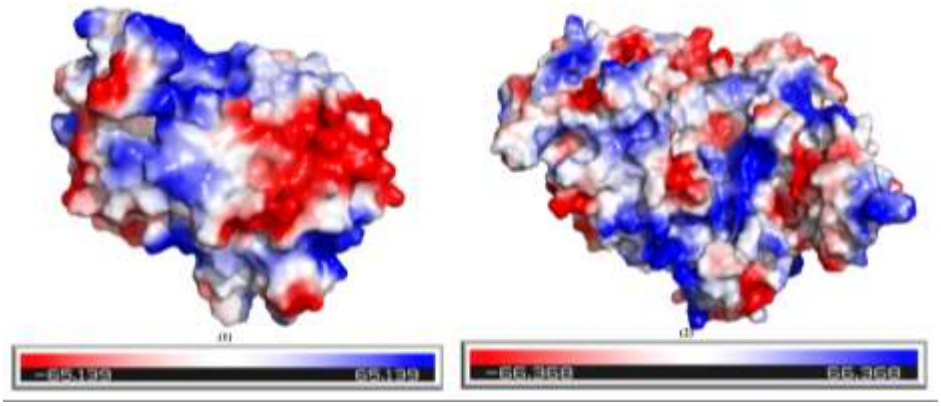

Figure 2. Electrostatic potential surface structure of receptor generated by PyMol v2.0.6 (1 = 5ZJ6 and 2 = 6AUI)

Preparation of ligands for docking

The ligand preparation involved building of 2D structure using Chem-Draw professional v15.1 and energy minimization through Chem3D professional v15.1 MMFF (Merck Molecular Force Field), using the job type: Minimum RMS Gradient of 0.010 kcal/mol and RMS distance of 0.1 Å, and saved as a .mol file. Structure validation and optimization was also performed with the help of Gaussian 9W and Gauss View v6.0.

Docking and Display of the results

Collaborative docking was performed to dock one ligand at a time through the following steps-(1) Click on menu run/run AutoGrid/run AutoDock, check job status after completion of docking a .dlg file is automatically generated.
(2) Click Docking/Browse/.dlg file, click Conformations/Play/&/Show info, the algorithm searches the overall lowest energy function of ligand from the saved minimum energy conformations with the help of genetic and stochastic global optimization.

iGEMDOCK

Optimized PDB files of the receptor and ligands were prepared, ligand conformations and orientation comparative to the binding site of receptor based on generic algorithm (GA) method were analyzed to produce receptor-ligand interactions [28]. Accurate docking (very slow docking) was performed and the docking parameters were set as follows: population size: 800, generations: 80, number of solutions: 10. After completion of docking, the best docking pose was generated having minimum binding energy [29]. The observed scoring function of iGEMDOCK is assessed as:

$$Fitness = vdW + Hbond + Elec \quad (2)$$

where,
vdW = van der Waals energy, *H bond* = hydrogen bonding energy and *Elec* = electrostatic energy, respectively. Finally, iGEMDOCK post-analysis tool was used to visualize the docked poses.

Computer-aided pharmacokinetics studies

SwissADME was used for pharmacokinetic studies and OSIRIS data warrior v4.6.2 was used to estimate the toxicity of the compounds. The metabolic sites in the compounds were predicted using MetaPrint2D in Bioclipse v2.6.2. Molinspiration v2016.03 was used to calculate the bioactivity score and admetSAR was used to analyze the ADMET properties.

Metabolic transformation prediction

MetaPrint2D is used to predict the metabolic sites and analyzes the results by computing normalized occurrence ratio (NOR) [30]. A high NOR value specifies a common site found in the metabolite database. The metabolized sites are shown by different colors; Red: High, Orange: Medium, Green: Low, White: Very low and Grey: No data, as shown in Table 1.

Molecular parameters

The molecular properties including LogP, topological polar surface area (TPSA), number of hydrogen bond donors (OHNH) and hydrogen bond acceptors (ON), rotatable bonds (RB), molar refractivity (MR) molecular weight (MW) and percentage of absorption (% of ABS) were computed using SwissADME.

Assessment of Druglikeness

Druglikeness of the proposed compounds was assessed using the following filtering rules:

Lipinski's rule-of-five

According to the rule-of-five, for good oral absorbance, a compound must have hydrogen bond acceptors (10≥ON), hydrogen bond donors (5≥OHNH), calculated LogP (5≥cLogP), rotatable bonds (10≥RB) and molecular weight (500≥MW) with a maximum of one violation.

Leadlikeness

According to Teague et al., (1999) compounds with MW in the range 250-350, a XLOGP3 value of <3.5 and <7 rotatable bonds satisfy the criteria for lead-likeness. When the lead is an agonist, the ED_{50} is taken to be a maximal value for the affinity of the molecule having the following desirable properties: MW<350 and cLogP<3 [31].

ADMET prediction

ADMET properties including (i) Brain/blood penetration coefficient (ii) Human Intestinal Absorption (iii) Caco-2 cell permeability (iv) Prediction of IC_{50} values for rat model (v) Ames toxicity and (vi) Carcinogenic effect of the proposed compounds were studied using the admetSAR server [32].

Toxicity potential assessment

The toxicity risk of the proposed compounds was assessed by means of a pre-computed set of structural fragments. Toxic parameters of the proposed compounds were predicted by OSIRIS Data Warrior Software [33].

Bioactivity score prediction

Using Molinspiration, the bioactivity scores of the proposed compounds against regular human receptors were calculated [34]. Larger the bioactivity score, greater is the probability of the compound to be active. A molecule having a bioactivity score more than 0.0 is most likely to be biologically active, while values ranging from -5.0 to 0.0 are for moderately active compounds and if the score is less than -5.0, the compound is expected to be inactive [35].

Results and Discussion

Chemistry

The synthetic procedure is illustrated in scheme 1. Grinding malononitrile with the appropriate 2,4-dichlorobenzaldehyde/Isatin derivative in the presence of PEG-400 as a solvent afforded the 2-benzylidene/2-(2-oxo-indolin-3-ylidene) malononitrile derivative (C1/C8) as previously reported [36–40].

Grinding of 2,4-dichlorobenzaldehyde with malononitrile at room temperature for 10 minutes in the absence of solvent gave product in low yield in the case of C1 and C8. When the Knoevenagel condensation was carried out in PEG-400 with grinding for 10 minutes the adduct C1 was obtained in 75% yield**.** High viscosity of PEG-400 caused the product to be obtained in low yield. If grinding was done using a mixture of PEG-400 and water (1:1) as solvents at RT, C1 was obtained in high yield (99%). The yield of the product was dependent on the solvent used **(Table 2)**.

Table 2. Optimization of synthesis of compound C1-C7 and C8-C12 *via* the Knoevenagel condensation using PEG-400 and water as solvents in grinding method

Entry	Time (min)	Solvents	Product	Yield (%)
1	10	-	C1	Trace
2	10	PEG-400	C1	75
3	10	water	C1	69
4	**10**	**PEG-400/water**	**C1**	**99***
5	5	PEG-400/water	C1	89
6	10	-	C8	Trace
7	10	PEG-400	C8	90
8	10	water	C8	89
9	**10**	**PEG-400/water**	**C8**	**99****
10	5	PE400/water	C8	88

* Most suitable optimized condition for 2-benzylidene malononitrile derivatives

** Most suitable optimized condition for 2-(2-oxo-indolin-3-ylidene) malononitrile derivatives

Experimental investigation revealed that grinding with organic solvents in a glass pestle and mortar favors condensation and dehydration reaction [13]. To the best of our knowledge, this is the first report where Knoevenagel condensation took place by grinding in the presence of PEG-400 at RT and in the absence of a catalyst. The proposed synthetic procedure involved isaldol addition facilitated by a polar solvent **(Figure 3).** The proposed reaction mechanism was also optimized with the help of DFT and also explained in terms of dual

descriptor (Δf(r)) [41]. The value of Δf(r)>0 supports nucleophilic attack while Δf(r)<0 favors electrophilic attack (**Supplementary Table 1**). The reaction mechanism was supported by Δf(r) [41,42]. Initially, active methylene compound malononitrile (I) undergoes tautomerism, which is favored by the presence of two adjacent nitrogen atoms (Δf(r) = -0.7157 eV, electrophilic) and activated hydrogen atoms ((Δf(r) = -0.7374 eV, nucleophilic). A highly reactive tautomer intermediate 3-iminoacrylonitrile (II) is formed and activated methylene carbon atom becomes suitable for the electrophilic attack (Δf(r) = -8.4820 eV, electrophilic). On the other hand, aldehyde (III) α, β di-one or isatin (VI) in the presence of proton (protic solvent) develops intermediate IV/VII with oxonium ion ($C=OH^+$) and converts into intermediate V/VIII. Due to instability and high reactivity, it proceeds, through a 1,2-elimination leading to the formation of a double bond and removal of a water molecule. Moreover, IR spectra of the compounds (C1-C12) revealed a sharp characteristic stretching absorption band at 2227-2235 cm^{-1} corresponding to CN group. Aromatic C=C absorbance was obtained between 1689-1602 cm^{-1}. The band corresponding to the =CH aromatic group was found between 3086-3057 cm^{-1}. The ^1H NMR spectra revealed a singlet assigned to CH protons at 8.12-7.75 ppm. ^{13}C NMR and mass spectra also confirmed the structure of synthesized compounds.

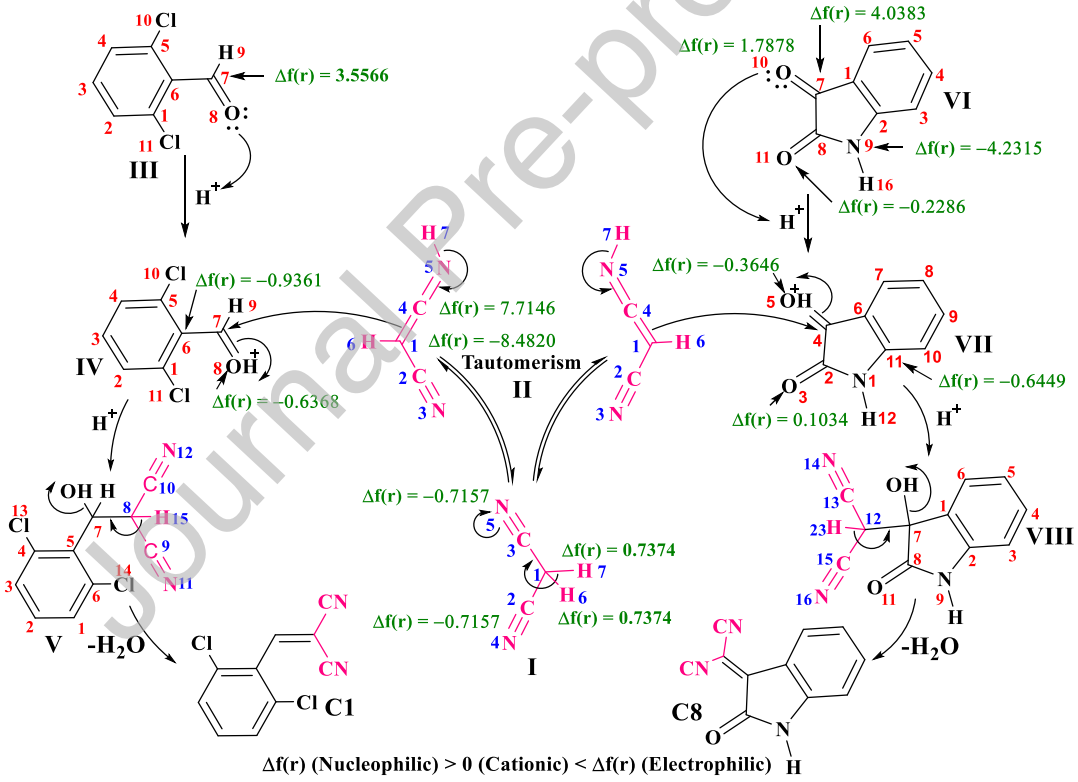

Figure 3. The plausible comparative (aldehyde and ketone) reaction mechanism of Knoevenagel condensation in the presence of proton and in terms of (eV) of dual descriptor ($\Delta f(r)$)

DFT calculations

Optimized geometry

The thermodynamically favored geometry and optimized structural constraints such as bond length, bond angle and dihedral angles were also calculated. The optimized structures are

shown in **Figure 4** and parameters are presented in Supplementary tables 10-11. From the structural parameters, the calculated distances between different C–C bonds of the ring carbon and active methylene group carbon atoms were found to be approximately same and correlated with the available experimental data. Different functional groups attached with the ring influenced the slight change in the optimized parameters as presented in the Supplementary tables 10-11.

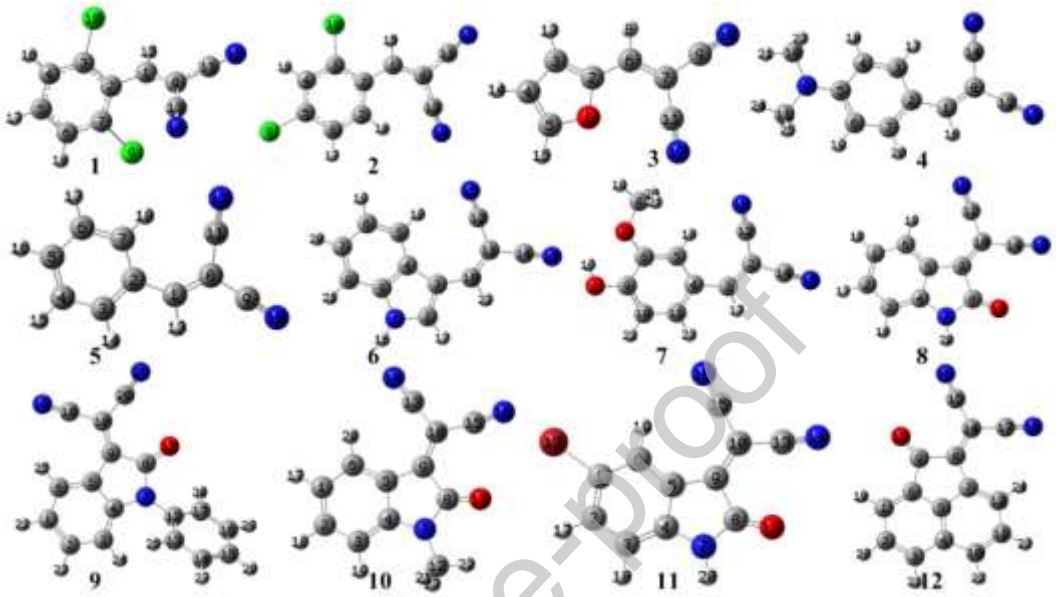

Figure 4. The ball-and-stick model of optimized structures of alkylidenemalononitrile derivatives (C1-C12) with atom numbering scheme

Vibrational frequency analysis

The number of normal modes of vibration and their classification into stretching, bending, torsion and out of plane modes along with total number of atoms and electrons are given in **Tables 3-4.** The potential energy distribution (PED) analyses were also performed to evaluate the vibrational frequencies of each compound [43]. The experimental and theoretical infrared spectra of all the alkylidenemalononitrile derivatives (C1-C12) are shown in **Figure 5.** The theoretical vibrational frequencies were computed in the gaseous phase, whereas the experimental values were obtained in solid phase. Theoretical spectra were scaled by 0.9679 [44], both the experimental and theoretical spectral studies were done between 4000-450 cm^{-1}. Good correlation was obtained between the experimental and theoretical infrared spectra.

Table 3. Showing the general findings of vibrational frequency analysis obtained from DFT/B3LYP/6-31G(d,p) level

	Compounds											
	C1	**C2**	**C3**	**C4**	**C5**	**C6**	**C7**	**C8**	**C9**	**C10**	**C11**	**C12**
TMV	48	48	39	72	48	60	63	54	84	63	54	66
TA	18	18	15	25	18	22	23	20	30	23	20	24
TE	112	112	74	104	80	100	104	100	140	108	134	118
STRE	17	17	14	25	17	21	22	19	29	22	19	23
BEND	16	16	13	24	16	20	21	18	28	21	18	22
TORS	11	11	10	19	13	16	16	12	21	14	12	15
OUT	4	4	2	4	2	3	4	5	6	6	5	6

TMV: Total mode of vibrations
TA: Total atoms
TE: Total electrons
STRE: Stretching vibration mode
BEND: Bending vibration mode
TORS: Torsion vibration mode

OUT: Out of plane vibration

Ring vibration

C–H stretching vibrations were associated with ring and active methylene group. The C-H stretching vibrations in the phenyl ring occurred between 3100-3000 cm^{-1} [45]. Substitution sites and their properties did not affect the aromatic C–H stretching vibration region while ortho disubstituted aromatic ring caused a strong absorption band at 750 cm^{-1}. The theoretical =C-H out of plane absorbance was obtained at 922-690 cm^{-1} for aromatic ring. Similarly, in-plane C-H bending was found between 1300-1000 cm^{-1} and aromatic C=C absorbance bands were obtained at 1600 and 1475 cm^{-1} [46] **(Table 3)**. The experimental ring vibrations were found between 1452-1610 cm^{-1} whereas the theoretical observations were between 1438-1632 cm^{-1} as shown in **Figure 5.** All the theoretical and experimental findings were in good agreement with each other.

C-H vibrations

The alkene C-H stretching vibration was observed in the range 3300-2750 cm^{-1}, =C-H sp^2 absorbance band was found near ~3100 cm^{-1} [46]. The =C-H out of plane vibration was observed between 1000-650 cm^{-1} and used to define the degree of substitution on the double bond C=C (1660-1600 cm^{-1}). An overtone or combination weak band was obtained at 2000 cm^{-1} and 1667 cm^{-1}. On the other hand for 1,2,4 substitution, a medium band was observed at 900 cm^{-1} and at 800 cm^{-1}, a strong band was also obtained [47] (**Table 4 and Figure 5)**.

C–Cl vibration

The stretching vibration mode of ring C–Cl bond was obtained between 760–505 cm^{-1} [47]. The C-Cl stretching vibrations bands were observed at 759 and 780 cm^{-1} for compound C1 and C2 theoretically whereas the experimental bands were obtained at 772 and 793 cm^{-1}. Inductive effect as well as vibrational coupling with other groups such as C=N was responsible for slightly higher absorption of C–Cl bond.
In general the C≡N stretching vibration is found at 2260-2240 cm^{-1} in saturated C≡N or in unsaturated C≡N, where conjugation is not found between the C≡N and the C=C group [46]. In a conjugated system, C≡N stretching vibration band shifts towards lower frequency range ~2232-2215 cm^{-1} [47]. In malononitrile derivatives, two C≡N groups were linked to the same C=C group, therefore, the symmetrical C≡N stretching vibration was found at 2235-2205 cm^{-1} whereas, the theoretical stretching vibration was obtained between 2282-2263 cm^{-1}. The variation may be due to the conjugation of the bond. The C≡N out-of-plane torsion was expected at 454 cm^{-1} [47]. PED analysis also supported the experimental observations.

C–N vibration

The identification of the C–N stretching vibration mode in fingerprint region is very challenging, because the vibration band overlaps with other core vibrations. The C–N stretching vibrations appeared between 1382-1266 cm^{-1} as reported in literature [25]. The theoretical and experimental observation showed good correlation with each other. The low PED values showed that C–N vibration bands overlapped with some other vibrations as well.

O–H vibrations

The hydrogen bonded broad peaks of O–H vibrations were obtained between 3400–3300 cm^{-1}. While, non-hydrogen bonded O–H stretch vibrations appeared as sharp and weak bands between 3650-3600 cm^{-1} [47]. The C-O-H bending band is reportedly observed in the finger

printing region 1440-1220 cm^{-1} along with the C-O stretching band between 1260-1000 cm^{-1} [46,47]. Only compound C7 possessed hydroxyl group and the theoretical band was calculated at 3626 cm^{-1} under gaseous phase whereas the theoretical band in solid phase was found at 3403 cm^{-1}. Thus, it was concluded that theoretical O–H stretching vibration is non-hydrogen bonded while experimental findings were influenced by hydrogen bonding. 100% PED contribution also showed good agreement with the experimental data **Figure 5.**

C=O vibrations

The characteristic carbonyl group vibration absorption frequencies were observed between 1870-1540 cm^{-1}. The C=O stretching vibration of ketone with five-membered ring is generally reported at ~1751 cm^{-1}. Presence of α, β double bond shifts the typical C=O stretching band from 1751 cm^{-1} to a lower frequency viz. ~1730-1700 cm^{-1} [46]. The C=O stretching sharp band was observed in the experimental spectra at 1712, 1712, 1720, 1727 and 1720 cm^{-1} for compounds C8-C12. While, in the theoretical spectra C=O stretching band was observed at 1774, 1755, 1755, 1774 and 1755 cm^{-1}. The difference between the experimental and the theoretical bands may be attributed to the conjugation of C=O bonds, which is probably responsible for the lower stretching frequency.

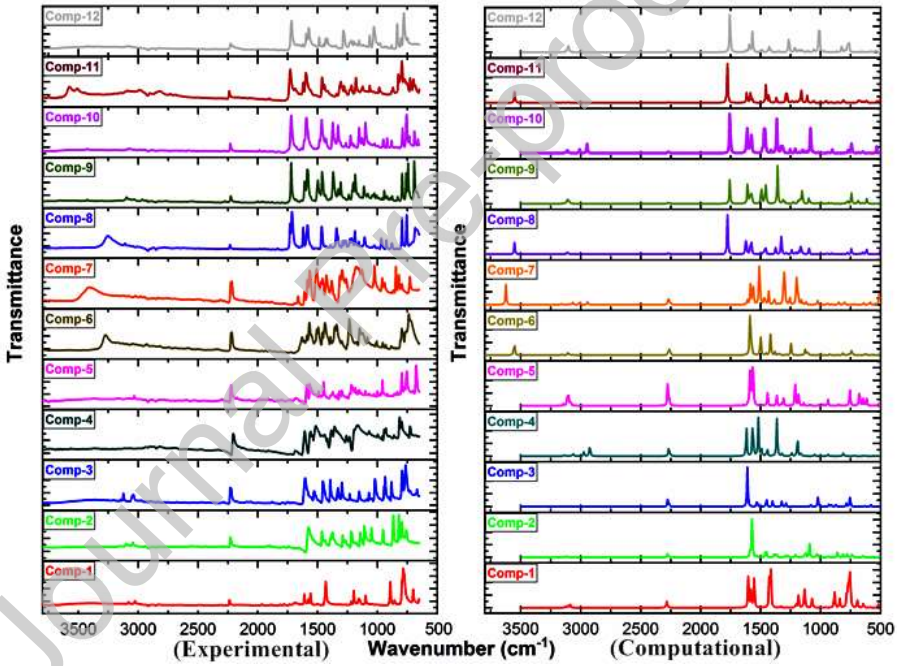

Figure 5. The experimental and theoretical IR spectra of all the synthesized compounds C1-C12

Table 4. Some anharmonic frequencies (cm^{-1}) of all the synthesized compounds C1-C12 at DFT/B3LYP/6-31G(d,p) level in gaseous phase

	Compounds											
	C1	**C2**	**C3**	**C4**	**C5**	**C6**	**C7**	**C8**	**C9**	**C10**	**C11**	**C12**
	Theoretical Vibrational Frequencies											
$\upsilon_{C\equiv N}$	2282	2276	2275	2268	2275	2263	2264	2272	2268	2274	2272	2275
υ_{C-H} **(ali.)**	3129	3148	3192	3060	3143	3154	3064	-	-	-	-	-
υ_{C-H} **(aro.)**	3087	3116	3162	2975	3100	3109	3008	3112	3109	3115	3102	3102
υ_{O-H}	-	-	-	-	-	-	3626	-	-	-	-	-
υ_{C-Cl}	759	780	-	-	-	-	-	-	-	-	-	-
$\upsilon_{C=O}$	-	-	-	-	-	-	-	1774	1755	1755	1774	1755
$\upsilon_{C=C}$ **(aro.)**	1603	1572	1608	1617	1589	1585	1585	1576	1608	1608	1614	1596
υ_{N-H}	-	-	-	-	-	3551	-	3549	-	-	3549	-
	Experimental Vibrational Frequencies											
$\upsilon_{C\equiv N}$	2238	2227	2227	2205	2227	2220	2227	2235	2227	2235	2235	2227
υ_{C-H} **(ali.)**	3086	3102	3124	2935	3151	3051	3027	-	-	-	-	-

υ_{C-H} **(aro.)**	3024	3050	3043	2905	3028	2931	2977	3109	3094	3028	3097	3086
υ_{O-H}	-	-	-	-	-	-	3403	-	-	-	-	-
υ_{C-Cl}	772	793	-	-	-	-	-	-	-	-	-	-
$\upsilon_{C=O}$	-	-	-	-	-	-	-	1712	1712	1720	1727	1720
$\upsilon_{C=C}$ **(aro.)**	1612	1602	1603	1610	1595	1624	1617	1617	1610	1611	1621	1595
υ_{N-H}	-	-	-	-	-	3271	-	3256	-	-	3573	-

NMR spectral analysis

The gauge including atomic orbital (GIAO) method was used to calculate theoretical chemical shifts values. The ^{13}C and ^{1}H chemical shifts were scaled δ = (intercept - isotropic magnetic shielding)/slope; where the values of intercept and slope were 188.57 and 0.94, respectively, for ^{13}C spectral calculation and 31.54 and 1.03, respectively for ^{1}H spectral calculation [48]. Unscaled chemical shifts were calculated at the same level of theory with reference to tetramethylsilane (TMS). The ^{13}C chemical shifts were designated in $CDCl_3$ for C1-C7 and DMSO for C8-C12. The experimental ^{13}C and ^{1}H NMR spectra of synthesized compounds C1-C12 have been shown in Supplementary information. The calculated ^{13}C and ^{1}H scaled chemical shift values have been shown in the Supplementary Table 12 & 13. ^{13}C chemical shifts values were found in the range of 110-175 and 100-150 ppm [47]. The chemical shift of =CH- group was deshielded, due to the presence of adjacent strong electrophilic carbon in two nitrile groups and observed at ≤100 ppm in the theoretical as well as experimental spectra. The electrophilic carbon of nitrile (C≡N) group was found near 110-140 ppm, due to the presence of two adjacent C≡N groups, they were slightly deshielded and the chemical shift was observed at ~100 ppm. The average correlation (R) of theoretical as well as experimental ^{13}C chemical shifts for C1-C12 was 0.977. The alkylidenemalononitrile derivatives mainly possessed activated double bonded hydrogen =CH. The ^{1}H chemical shift value of =CH was strongly shielded due to the presence of two adjacent nitrile groups and resonance due to the aromatic ring and found between 6.4-8.5 ppm in the theoretical while between 6.7-8.1 ppm in the experimental spectra. The theoretical and experimental values for =CH- chemical shifts showed good correlation supporting the Knoevenagel condensation. The average correlation coefficient value (0.934) of the theoretical and experimental ^{1}H chemical shift of all the compounds showed good agreement, except for the NH group. This variation may be due to the presence of hydrogen bonding that leads to strong shielding of the NH peak, but experimental chemical shift of NH proton was observed as reported in literature [25].

Electronic absorption spectral analysis

The UV-Vis spectra are observed due to electronic transition from bonding molecular orbitals (BMOs) to anti-bonding molecular orbital (ABMOs). The UV-visible spectra of all compounds *viz.* C1-C12 were calculated in gaseous as well as in $CHCl_3$ (C1-C7) and DMSO (C8-C12), by using optimized structures. The comparison of computed UV-Vis spectra in gaseous and solvent phases in $CHCl_3$ (C1-C7) and DMSO (C8-C12) are represented in **Figure 6.** The UV-Vis spectral findings are shown in Supplementary Table 18. The correlation (0.9707) between theoretical and experimental UV-Vis spectra was in good correlation with each other (**Figure 6**). All the synthesized compounds illustrated H→L transition with major contribution between 59-99% in gaseous phase while 61-99% in solvent phase. The molecular orbital plots and coefficients showed that the frontier molecular orbitals had more *p* character. Therefore, the main electronic transition was π→π*.

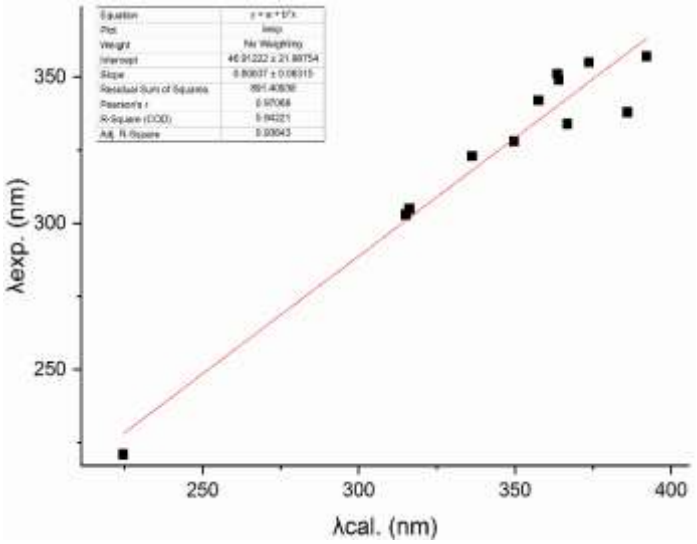

Figure 6. The computed UV-Vis spectra of all synthesized compounds C1-C12

Thermodynamic properties analysis

The thermodynamic properties such as molar capacity, electronic energy (EE), zero point vibrational (ZPV) energy, rotational constants (RC) and rotational temperature (RT) were computed for all the synthesized compounds [49]. The statistical thermochemical investigation was done at ambient temperature (298.15 K) and one atmospheric pressure. All the statistical thermodynamic findings were used to calculate other thermodynamic properties such as entropy (S), zero-point energy (ZPE), heat capacity (C), enthalpy (H) and Gibbs free energy (G) represented in **Table 5.**

Table 5. The computed thermodynamic parameters of all synthesized compounds C1-C12

Parameter	C1	C2	C3	C4	C5	C6	C7	C8	C9	C10	C11	C12
ZPVE (Kcal/Mol)	70.06	70.433	128.57	63.53	82.65	101.30	106.06	85.709	136.27	103.37	79.28	104.38
	0.670	0.897	1.661	2.498	2.080	1.238	1.122	1.045	0.507	0.789	0.770	0.749
RC (GHz)	0.473	0.296	0.259	0.695	0.542	0.389	0.348	0.512	0.237	0.494	0.230	0.366
	0.320	0.223	0.224	0.544	0.430	0.296	0.266	0.344	0.168	0.305	0.177	0.246
	0.032	0.043	0.080	0.120	0.100	0.059	0.054	0.050	0.024	0.038	0.037	0.036
RT (Kelvin)	0.023	0.014	0.012	0.033	0.026	0.019	0.017	0.025	0.011	0.024	0.011	0.018
	0.015	0.011	0.010	0.026	0.021	0.014	0.013	0.017	0.008	0.015	0.009	0.012
					S (Cal/Mol-Kelvin)							
Total	113.86	116.38	122.75	95.85	100.15	110.18	117.57	107.61	131.86	114.88	117.52	114.88
Translational	42.095	42.095	41.741	40.806	41.006	41.68	41.79	41.709	42.691	41.92	42.711	42.201
Rotational	32.429	32.962	32.479	30.210	30.872	32.09	32.402	31.836	34.031	32.27	33.590	32.835
Vibrational	39.331	41.319	48.526	24.839	28.268	36.41	43.39	34.060	55.137	40.70	41.217	39.846
					CV (Cal/Mol-Kelvin)							
Total	44.98	44.713	52.56	32.99	37.01	45.80	50.426	44.845	63.500	49.996	49.054	51.950
Translational	2.981	2.981	2.981	2.981	2.981	2.981	2.981	2.981	2.981	2.981	2.981	2.981
Rotational	2.981	2.981	2.981	2.981	2.981	2.981	2.981	2.981	2.981	2.981	2.981	2.981
Vibrational	39.015	38.752	46.60	27.03	31.04	39.84	44.464	38.883	57.539	44.034	43.092	45.989
					E (KCal/Mol)							
Total	77.93	78.271	137.67	69.301	88.924	108.77	114.64	93.117	146.60	111.78	87.646	112.73
Translational	0.889	0.889	0.889	0.889	0.889	0.889	0.889	0.889	0.889	0.889	0.889	0.889
Rotational	0.889	0.889	0.889	0.889	0.889	0.889	0.889	0.889	0.889	0.889	0.889	0.889
Vibrational	76.155	76.493	135.91	67.523	87.147	106.99	112.86	91.339	144.83	109.99	85.868	110.95
μ (Debye)	6.42	4.93	7.45	11.05	6.64	9.62	6.31	8.15	8.38	8.25	7.42	8.64
α (a.u.)	133.39	150.48	105.48	176.68	121.03	151.43	149.51	140.79	206.61	153.32	161.41	178.62
EE (a.u.)	-1413.31	-1413.32	-491.91	-628.12	-494.14	-625.72	-683.89	-661.63	-892.69	-700.95	-3232.73	-759.90
S (cal/mol-kelvin)	113.86	116.38	95.85	122.75	100.15	110.18	117.57	107.61	131.86	114.88	117.52	114.88
Cv (cal/mol-kelvin)	44.98	44.71	32.99	52.56	37.01	45.80	50.43	44.85	63.50	50.00	49.05	51.95
E (Thermal) Kcal/mol	77.93	78.27	69.30	137.69	88.92	108.77	114.63	93.12	146.61	11.78	87.65	112.73

G (au)	0.07	0.07	0.07	0.16	0.10	0.12	0.13	0.10	0.17	0.12	0.09	0.13
ZPE (au)	0.11	0.11	0.10	0.21	0.13	0.16	0.17	0.14	0.22	0.17	0.13	0.17

FMO (Frontier Molecular Orbital) analysis

The electron donating capability is illustrated by E_{HOMO}, whereas the electron accepting capability is illustrated by E_{LUMO} and the E_{GAP} between HOMO and LUMO describes the stability of the molecular system and elucidates the subsequent charge transfer relations occurring within the molecular system. E_{HOMO} is also associated with the ionization potential (IP) and E_{LUMO} is related to electron affinity (EA) [25]. The small value of E_{GAP} favors the biological activity of the compound. The E_{HOMO} and E_{LUMO} were computed in gaseous and solvent phase (compound C1-C7 in $CHCl_3$ and C8-C12 in DMSO) using IEFPCM model. The value of E_{GAP} for all the compounds was between 4.812-4-4.671 eV in gaseous and solvent phase while for C1, it was -2.898 and -2.736 eV which was lowest for C9 in gas and solvent phase. 2-benzylidene malononitrile derivatives (C1-C7) possessed highest value of E_{GAP} between 4.812 eV (in gas) and 4.671 eV (in solvent) which was highest for compound C1, whereas 3.621 eV (in gaseous) and 3.552 eV (in solvent) which was lowest for compound C4, showing highest stability with least reactivity as compared to 2-(2-oxo-indolin-3-ylidene) malononitrile derivatives (C8-C12), possessing E_{GAP} between 3.291 eV (in gaseous) and 3.072 eV (in solvent) and highest for C12, 2.898 eV (in gas) and 2.736 eV (in solvent) lowest for compound C9 as represented in **Table 6 and Figure 7.** 2-(2-oxo-indolin-3-ylidene) malononitrile derivatives (C8-C12) showed least stability with high reactivity. Experimentally, it was found that 2-(2-oxo-indolin-3-ylidene) malononitrile derivatives (C8-C12) were formed feasibly with high yield as compared to the 2-benzylidene malononitrile derivatives (C1-C12). In the HOMO and LUMO plots, positive phase was represented by red and negative phase was represented by green color as shown in **Figure 8.**

Table 6. HOMO-LUMO energies with HOMO-LUMO energy gap

(eV)	Phase	C1	C2	C3	C4	C5	C6	C7	C8	C9	C10	C11	C12
E_{HOMO}	**Gas**	-7.351	-7.244	-6.941	-6.076	-7.073	-6.152	-6.291	-6.750	-6.442	-6.585	-6.729	-6.786
	Solvent	-7.161	-7.076	-6.767	-5.955	-6.955	-6.055	-6.168	-6.473	-6.279	-6.358	-6.435	-6.546
E_{LUMO}	**Gas**	-2.545	-3.052	-2.645	-2.455	-2.916	-2.288	-2.643	-3.591	-3.544	-3.531	-3.791	-3.495
	Solvent	-2.490	-2.880	-2.527	-2.403	-2.798	-2.220	-2.582	-3.502	-3.543	-3.489	-3.636	-3.474
E_{GAP}	**Gas**	4.812	4.192	4.296	3.621	4.157	3.864	3.648	3.165	2.898	3.054	2.938	3.291
	Solvent	4.671	4.196	4.240	3.552	4.157	3.835	3.586	2.971	2.736	2.869	2.799	3.072

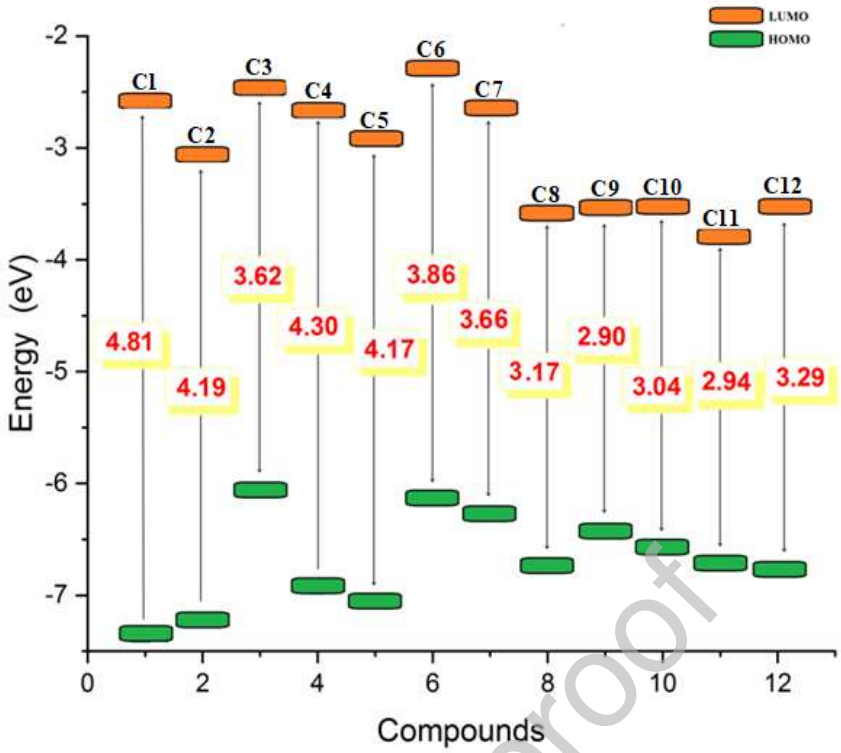

Figure 7. Energy level graph of E_{HOMO}, E_{LUMO} and E_{GAP} for all the synthesized compounds C1-C12

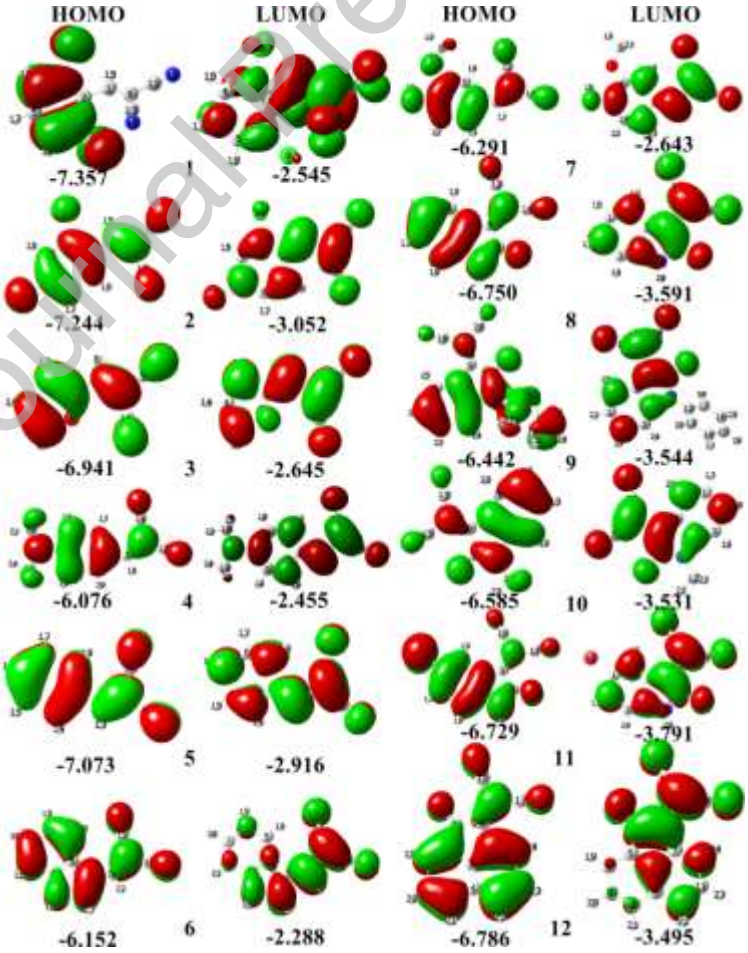

Figure 8. The HOMO and LUMO plots for all the synthesized compounds C1-C12 computed by TD-DFT/B3LYP/6-31G(d,p) method.

Molecular electrostatic potential (MEP) analysis

The molecular electrostatic potential explores the charge distribution and polarization along with the hydrogen bonding capability and reactivity of the molecular system. MEP also elucidates complete information of the electrophilic and nucleophilic sites in the molecular system, thereby providing statistical polarity of the molecule in a pictorial form, to recognize the polar and nonpolar sites of the molecule in color variations as shown in the **Figure 9.** The red color characterizes electrophilic reactivity (most negative), blue color characterizes nucleophilic reactivity (most positive) and green color generally illustrates nonreactive sites (zero electrostatic potential). MEP decreases in the order; blue>green>yellow>orange>red [52]. The color code (red to blue) of the compounds was found between -4.614 to 4.614 (C1), -4.640 to 4.640 (C2), -5.079 to 5.079 (C3), -5.909 to 5.909 (C4), -4.967 to 4.967 (C5), -8.303 to 8.303 (C6), -6.034 to 6.034 (C7), -7.252 to 7.252 (C8), -5.584 to 5.584 (C9), -5.548 to 5.548 (C10), -7.727 to 7.727 (C11) and -5.438 to 5.438 a.u. (C12), respectively**.** From the MEP plots it was concluded that nitrile group of alkylidenemalononitrile derivatives possessed high electropositive potential (red) and the activated double bond hydrogen (=CH-) possessed slightly low electropositive region (blue). Consequently, nitrile groups of alkylidenemalononitriles support electrophilicity while the presence of activated =CH- group favors nucleophilicity (**Figure 9).**

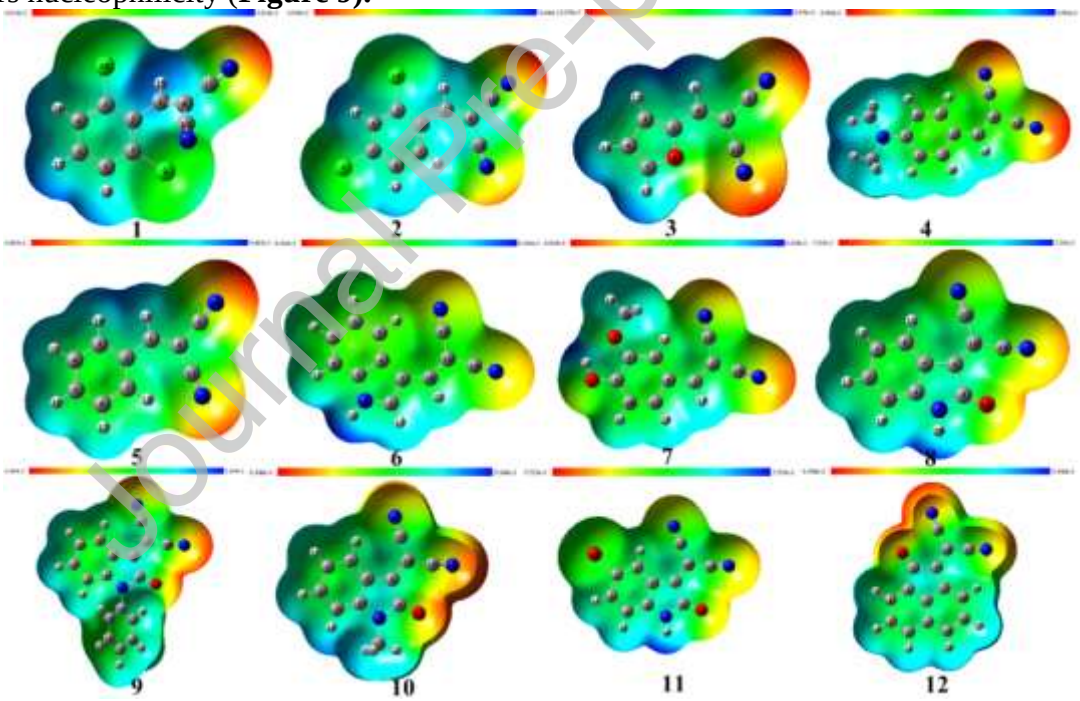

Figure 9. MEP formed by mapping of total density over electrostatic potential in gas phase for all the synthesized compounds C1-C12

Non-Linear Optical (NLO) properties

Larger value of hyperpolarizability of a molecular system favors NLO properties which can be explored for optoelectronics and for optical devices. Statistical evaluation of hyperpolarizability is quite advantageous for establishing a correlation among the molecular system as well as NLO properties [50]. Various NLO parameters including static dipole

moment (μ), mean polarizability (α_0), anisotropy of polarizability (Δα) and first hyperpolarizability (β_0) were calculated.

The values of the mean polarizability α_0 and the first hyperpolarizability β_0 were expressed in atomic units (a.u.) and converted into electrostatic units (esu) (α: 1 a.u. = 0.1482×10^{-24} esu and β: 1 a.u. = 8.6393×10^{-33} esu). The values of μ, α_0 Δα and β_0 for all the synthesized compounds are presented in **Table 8.** The calculated values of μ were 6.3921, 5.0228, 10.9961, 7.3570, 6.5609, 9.3780, 6.2581, 8.0757, 8.8739, 8.2803, 7.8269 and 8.7751 D (Debye), respectively for C1-C12. The highest value of μ was for C3 (10.9961 D). The calculated α_0 values for all the synthesized compounds were 16.2468×10^{-24}, 19.859×10^{-24}, 23.183×10^{-24}, 14.060×10^{-24}, 16.034×10^{-24}, 19.863×10^{-24}, 19.063×10^{-24}, 18.786×10^{-24}, 25.342×10^{-24}, 19.771×10^{-24}, 20.220×10^{-24} and 23.734×10^{-24} esu. The highest values of α_0 were for C9 and C3 *viz.* 25.342×10^{-24} and 23.183×10^{-24} esu. The value of first β_0 of all the compounds C1-C12 were 2.620×10^{-30}, 1.297×10^{-29}, 3.727×10^{-29}, 3.883×10^{-30}, 4.061×10^{-30}, 1.067×10^{-29}, 1.750×10^{-29}, 5.370×10^{-30}, 3.553×10^{-30}, 3.387×10^{-30}, 2.968×10^{-30} and 1.486×10^{-30} esu, respectively. The highest values of β_0 were for C3, C7, C2 and C6 *viz.* 3.727×10^{-29}, 1.750×10^{-29}, 1.297×10^{-29} and 1.067×10^{-29} esu as compared to other alkylidenemalononitrile derivatives. Urea ($\beta_0 = 0.1947 \times 10^{-30}$ esu) and para-nitro aniline ($\beta_0 = 1.426 \times 10^{-29}$ esu) were used as reference compounds. The value of the molecular β_0 is a significant factor in an NLO system. Compounds C1-C12 possessed 13, 67, 191, 20, 21, 55, 90, 28, 18, 17, 15 and 8 times greater β_0 value as compared to urea and compounds C3 and C7 had β_0 values 2.6 and 1.2 times greater than para-nitro aniline. Therefore, all the alkylidenemalononitrile derivatives are potential candidates to be used as NLO materials **(Table 7).**

Table 7. Total static dipole moment (μ), the mean polarizability (α_0), the anisotropy of the polarizability (Δα) and the first hyperpolarizability (β_0) of all the synthesized compounds C1-C12

NLO	C1	C2	C3	C4	C5	C6	C7	C8	C9	C10	C11	C12
						Debye						
μ_x	-6.2476	4.8239	10.8945	-6.9359	-6.3936	7.8748	6.2546	-7.9867	-5.8061	8.2205	-4.5352	-8.4323
μ_y	0.3069	1.3942	-1.4831	-2.4517	-1.4686	-5.0911	-0.1597	-1.1903	6.7084	0.9838	6.3774	2.4248
μ_z	-1.3158	0.1240	0.1551	0.0889	0.0999	0.1204	0.1341	0.1148	-0.1794	0.1385	0.1394	0.1362
μ_0^1	6.3921	5.0228	10.9961	7.3570	6.5609	9.3780	6.2581	8.0757	8.8739	8.2803	7.8269	8.7751
						$\times 10^{-24} esu$						
α_{xx}	26.9780	37.4387	48.0172	26.9124	30.2012	36.1097	34.9316	33.6664	42.2311	34.9301	36.4064	40.8088
α_{yy}	0.7034	-0.1879	0.0305	0.4881	0.0860	-0.7258	-1.5568	0.4564	-2.3357	-0.7783	-2.9731	-0.2503
α_{zz}	21.0589	22.3269	21.5026	14.7793	17.8145	24.2043	22.2881	22.2365	36.1295	25.1599	27.2259	30.6448
α_{xy}	-1.1249	-0.0003	-0.0001	-0.0012	0.0004	-0.0009	-0.0002	-0.0000	0.0938	0.0000	-0.0000	-0.0002
α_{yz}	-1.1375	0.0006	0.0001	-0.0007	0.0002	0.0004	-0.0005	-0.0000	1.6036	0.0000	0.0000	-0.0002
α_{zx}	11.2705	7.1430	9.0384	5.2067	5.7952	7.0150	7.7307	6.6929	13.5017	8.0772	0.0813	7.9632
α_0	16.2468	19.859	23.183	14.060	16.034	19.863	19.063	18.786	25.342	19.771	20.220	23.734
Δα	53.874	44.653	56.603	31.825	35.942	44.112	35.236	22.230	71.269	46.961	35.688	107.292
						$\times 10^{-33} esu$						
β_{xxx}	2175.59	-14373.7	-35583.5	6115.47	5440.94	-11504.6	-18668.6	6803.92	-2268.07	-6029.79	4652.64	4103.58
β_{xyy}	739.47	1266.06	-3229.83	-1870.28	-1063.96	-161.12	693.16	153.78	-383.99	1614.90	-3285.81	-2098.88
β_{xzz}	-448.71	228.83	1546.55	-377.01	-317.95	1024.66	514.74	-1621.59	4223.22	1520.48	1454.93	-529.13
β_{yyy}	-732.07	-1547.63	-66.46	-333.54	-112.29	-827.79	-1120.22	635.07	-2800.31	-1696.66	905.10	175.79
β_{yzz}	59.95	0.73	-12.94	12.19	-0.13	-7.50	18.84	-12.08	81.99	-2.45	6.15	1.71
β_{yxx}	-135.31	-1.54	-4.66	2.51	-1.43	-6.63	4.63	-26.87	-467.30	8.14	3.36	-10.46
β_{zzz}	71.86	-5.50	6.52	8.89	-10.85	-4.96	-11.97	-38.66	197.22	9.60	3.36	-25.49
β_{zxx}	101.06	48.13	503.20	-67.36	-34.69	50.95	-64.34	-25.85	-232.05	276.64	-108.38	-42.50
β_{zyy}	184.77	32.62	3.68	-6.14	-10.29	-44.11	176.33	15.81	-36.56	195.17	4.97	25.06
β_0	2619.682	12971.77	37270.41	3882.61	4061.00	10674.26	17495.43	5369.91	3552.72	3386.55	2967.97	1485.61

Chemical reactivity

Global reactivity descriptors

The most commonly utilized quantum chemical parameters for global reactivity descriptors are E_{HOMO}, E_{LUMO}, E_{GAP}, absolute softness (σ), absolute hardness (η), optical softness (σ_0), chemical potential (*CP*),absolute electronegativity (χ), additional electronic charges (ΔN_{max}) nucleophilicity index (*N*) and electrophilicity index (ω). According to Koopman's theorem, global reactivity trends are successfully calculated with the help of E_{HOMO} and E_{LUMO}. Electrophilicity index ω, a global reactivity index similar to *CP* and η were also calculated. Electrophilicity index (ω) and its calculation were described by Parr et al. for the reactivity of organic molecules. A single ω scale (ω > 1.5 eV (strong), ω = 1.5-0.8 eV (moderate) and ω < 0.8 eV (marginal) electrophiles) was developed showing higher value of ω favors high electrophilicity. Therefore, ω is a new standard of stabilization in energy when the system obtains a ΔN_{max} from the environment. The values of E_{HOMO}, E_{LUMO}, E_{GAP}, σ, η, *S*, *CP*, χ, ΔN_{max}, *N* and ω for all the synthesized alkylidenemalononitrile derivatives have been enlisted in **Table 8.**

Table 8. Calculated E_{HOMO}, E_{LUMO}, E_{GAP}, absolute softness (σ), absolute hardness (η), optical softness (σ_0), chemical potential (*CP*),absolute electronegativity (χ), additional electronic charges (ΔN_{max}) nucleophilicity index (*N*) and electrophilicity index (ω) for all the synthesized compounds C1-C12 at DFT/B3LYP/6-31G(d,p) level

	C1	C2	C3	C4	C5	C6	C7	C8	C9	C10	C11	C12
IP^I	7.357	7.244	6.941	6.076	7.073	6.152	6.291	6.750	6.442	6.585	6.729	6.786
EA^I	2.545	3.052	2.645	2.455	2.916	2.288	2.643	3.591	3.544	3.531	3.791	3.495
$E_{GAP}{}^I$	4.812	4.192	4.296	3.621	4.157	3.864	3.648	3.165	2.898	3.054	2.938	3.291
χ^I	4.951	5.148	4.793	4.266	4.995	4.220	4.467	5.171	4.993	5.058	5.260	5.141
CP^I	-4.951	-5.148	-4.793	-4.266	-4.995	-4.220	-4.467	-5.171	-4.993	-5.058	-5.260	-5.141
η^I	2.406	2.096	2.148	1.811	2.079	1.932	1.824	1.583	1.449	1.527	1.469	1.646
σ^I	0.416	0.477	0.466	0.552	0.481	0.518	0.548	0.632	0.690	0.655	0.681	0.608
$\sigma_0{}^{II}$	0.208	0.239	0.233	0.276	0.241	0.259	0.274	0.316	0.345	0.327	0.340	0.304
ω^I	5.094	6.322	5.348	5.025	6.001	4.609	5.470	8.447	8.603	8.377	9.417	8.029
N^{II}	0.196	0.158	0187	0.199	0.167	0.217	0.183	0.118	0.116	0.119	0.106	0.125
$\Delta N_{max}{}^I$	2.058	2.456	2.231	2.356	2.403	2.184	2.447	3.257	3.446	3.312	3.581	3.124

Local reactivity descriptors

The conventional chemical reactivity and site selectivity of molecular system are recognized with the help of Fukui function. Fukui functions are calculated for a large number of organic molecules [44]. Fukui function is denoted by *f(r).*

Fukui function is mainly associated with the electron density $(\rho(r))$ of the system to a change in the total number of electrons $\left(N = \int \rho(r)\,dr\right)$in the limitation of a constant external potential acting on an electron (v(r)). Finite difference calculation classified three variables Fukui function for a system $f^+(r)$, $f^o(r)$ and $f^-(r)$ (for nucleophilic, radical and electrophilic attack) from N, as effect of the discontinuity of the electron density [51].
In a molecular system, high value of $f^+(r)$for an atom represents most likely nucleophilic attack and high value of $f^-(r)$ refers to electrophilic attack. To describe the electrophilic and nucleophilic reactive region for the evaluation of the intermolecular reactivity, Roy et al.

[52] suggested the relative electrophilic local softness $\left(S_k^+\right)$, the nucleophilic local softness $\left(S_k^-\right)$ and the radical local softness $\left(S_k^o\right)$ descriptors for a k[th] atom.

Chattaraj et al. [53] also offered three global local electrophilicity indices $\left(\omega_k^o\omega_k^+\omega_k^-\right)$ to recognize the radical, electrophilic and nucleophilic region in reactivity and regio-selectivity evaluation based on Parr global electrophilicity index (ω) and Fukui functions $\left(f_k^o\, f_k^+\, f_k^-\right)$ Recently, a new dual descriptor $\left(\Delta f\left(r\right)\right)$ was suggested by Morrel et al. for the nucleophilicity and electrophilicity [54].

The statistical values of $\left(\Delta f\left(r\right)\right)$ are given on the scale of -1, 0 to 1. If $\left(\Delta f\left(r\right)>0\right)$, suggesting that the site is appropriate for nucleophilic attack and $\left(\Delta f\left(r\right)>0\right)$ shows almost no nucleophilic attack and a favorable electrophilic attack.

Local reactivity descriptors based on electron density such as Fukui function $\left(f_k^o\, f_k^+\, f_k^-\right)$, local electrophilicity indices $\left(\omega_k^o\omega_k^+\omega_k^-\right)$, local softness $\left(S_k^oS_k^+S_k^-\right)$ and dual descriptor $\left(\Delta f\left(r\right)>0\right)$ describe a specific region of the chemo- or regio-selectivity of a molecular system. The findings of Fukui function, local electrophilicity, local softness and dual descriptor indices of atoms of the all the synthesized compounds are given in **Table 9.**

Table 9. Using MPA, Fukui function, local softness, local electrophilicity and dual descriptor indices in eV for αC and βC

		C1	C2	C3	C4	C5	C6	C7	C8	C9	C10	C11	C12
q_{N+1}	αC	-4.7104	-2.9035	-2.3892	-4.2097	-2.7103	-3.8723	-3.8042	-2.2831	-3.1457	-2.5606	-2.5634	-2.6124
	βC	-4.2750	-2.3674	-4.0464	-3.2546	-1.8531	-3.2899	-3.0287	-1.4531	-1.4586	-1.4776	-1.5783	-0.7320
q_{N-1}	αC	-9.9977	-10.2099	-10.7242	-10.8984	-10.6072	-11.0127	-10.8957	-9.1187	-8.9908	-9.0861	-8.8820	-9.0752
	βC	-7.4534	-6.3839	-8.2398	-6.6125	-6.4601	-6.8493	-6.5608	-3.7172	-3.5593	-3.5811	-3.7417	-3.3335
q_N	αC	-6.2778	-6.8438	-7.1132	-7.9976	-7.1894	-7.9949	-7.7962	-5.4397	-5.4506	-5.4560	-5.2057	-5.5567
	βC	-2.3402	-2.5008	-4.0328	-2.3212	-2.1851	-2.5008	-2.2096	-0.2803	-0.1333	-0.0844	-0.3510	0.1007
f_k^+	αC	3.7199	3.3661	3.6110	2.8981	3.4151	3.0178	3.0994	3.6791	3.5430	3.6301	3.6763	3.5185
	βC	5.1131	3.8859	4.2043	4.2913	4.2750	4.3485	4.3512	3.4369	3.4260	3.4967	3.3906	3.4342
f_k^-	αC	1.5674	3.9403	4.7240	3.7879	4.4791	4.1226	3.9893	3.1539	2.3021	2.8954	2.6423	2.9443
	βC	-1.9348	0.1333	-0.0109	-0.9334	0.3320	-0.7891	-0.8191	-1.1728	-1.3252	-1.3933	-1.2300	-0.8300
f_k^0	αC	2.6423	3.6546	4.1689	3.3444	3.9485	3.5702	3.5457	3.4178	2.9226	3.2627	3.1593	3.2328
	βC	1.5892	2.0082	2.0980	1.6790	2.3021	1.7797	1.7661	1.1320	1.0504	1.0504	1.0803	1.3007
S_k^+	αC	22.2213	23.1792	25.4976	22.7003	22.3411	21.2526	23.1193	31.6884	33.2639	32.3496	34.0531	29.1958
	βC	30.5455	26.7576	29.6856	33.6123	27.9658	30.6271	32.4558	29.6039	32.1673	31.1632	31.4054	28.4964
S_k^-	αC	9.3636	27.1331	33.3565	29.6692	29.2992	29.0352	29.7563	27.1657	21.6145	25.8024	24.4745	24.4337
	βC	-11.5569	0.9170	-0.0762	-7.3119	2.1715	-5.5581	-6.1091	-10.1011	-12.4413	-12.4168	-11.3937	-6.8874
S_k^0	αC	15.7830	25.1657	29.4379	26.1943	25.8296	25.1466	26.4473	29.4379	27.4406	29.0760	29.2638	26.8256
	βC	9.4943	13.8291	14.8142	13.1516	15.0591	12.5338	13.1733	9.7501	9.8616	9.3609	10.0059	10.7923
w_k^+	αC	0.2286	0.2367	0.2041	0.1306	0.2041	0.1361	0.1606	0.2721	0.2640	0.2640	0.2966	0.2612
	βC	0.3157	0.2721	0.2367	0.1905	0.2558	0.1959	0.2259	0.2558	0.2531	0.2558	0.2721	0.2531
w_k^-	αC	0.0952	0.2748	0.2667	0.1687	0.2667	0.1850	0.2068	0.2340	0.1714	0.2095	0.2123	0.2177
	βC	-0.1197	0.0082	0.0000	-0.0408	0.0190	-0.0354	-0.0435	-0.0871	-0.0980	-0.1007	-0.0980	-0.0626
w_k^0	αC	0.2884	0.4735	0.4599	0.2912	0.4354	0.3021	0.3565	0.5306	0.4626	0.5034	0.5470	0.4789
	βC	0.1714	0.2585	0.2313	0.1442	0.2531	0.1497	0.1769	0.1769	0.1660	0.1606	0.1878	0.1932
$\Delta f(r)$	αC	2.1497	-0.5742	-1.1130	-0.0408	-1.0640	-1.1048	-0.8898	0.5252	1.2409	0.7347	1.0313	0.5742
	βC	3.1784	3.7525	4.1934	0.2340	3.9457	3.5593	3.5321	2.2640	2.1008	2.1008	2.1606	2.6042

The alkylidenemalononitrile derivatives were characterized by the presence of two nitrile groups and activated double bond ($-C_\beta = C_\alpha(CN)_2$). The Cα (alpha carbon) which is directly

attached with the two nitrile groups, in the presence of high electronegativity nitrogen atom becomes partially positive and attracts the electrons of the bond and Cβ (beta carbon) becomes partially positively charged. Thus, Cβ becomes more suitable for the nucleophilic attack. The value of f_k^+ Cβ is higher for compound C1-C7 (2-benzylidene malononitrile derivatives) which was between 3.8859-5.11313 eV as compared to Cα which was between 2.8981-3.7199 eV. But in compounds C8-C12 (2-(2-oxo-indolin-3-ylidene) malononitrile derivatives), the value of f_k^+ Cβ is slightly lower (3.3906-3.4967 eV) as compared to Cα (3.5185-3.6791 eV) as shown in Supplementary Table 11. Thus, in this case it refers to electrophilic attack. These variations are due to the presence of active hydrogen on Cβ (compound C1-C7) and Cβ in ring (compound C8-C12). Furthermore, the value of $\left(\Delta f\left(r\right)\right)$ supports nucleophilic attack at Cβ for all the compounds (C1-C12). Finally, it was found that Cβ principal reactivity nucleophilic site is related to the electrophilic and radical attack **Figure 10 & 11.**

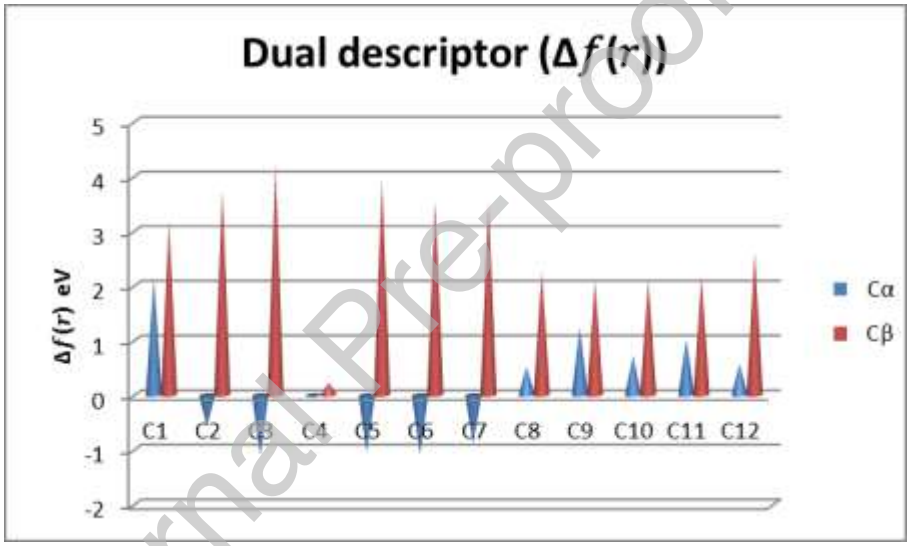

Figure 10. Comparison of dual descriptor $(\Delta f(r))$ values in eV for Cα and Cβ in all synthesized compounds C1-C12

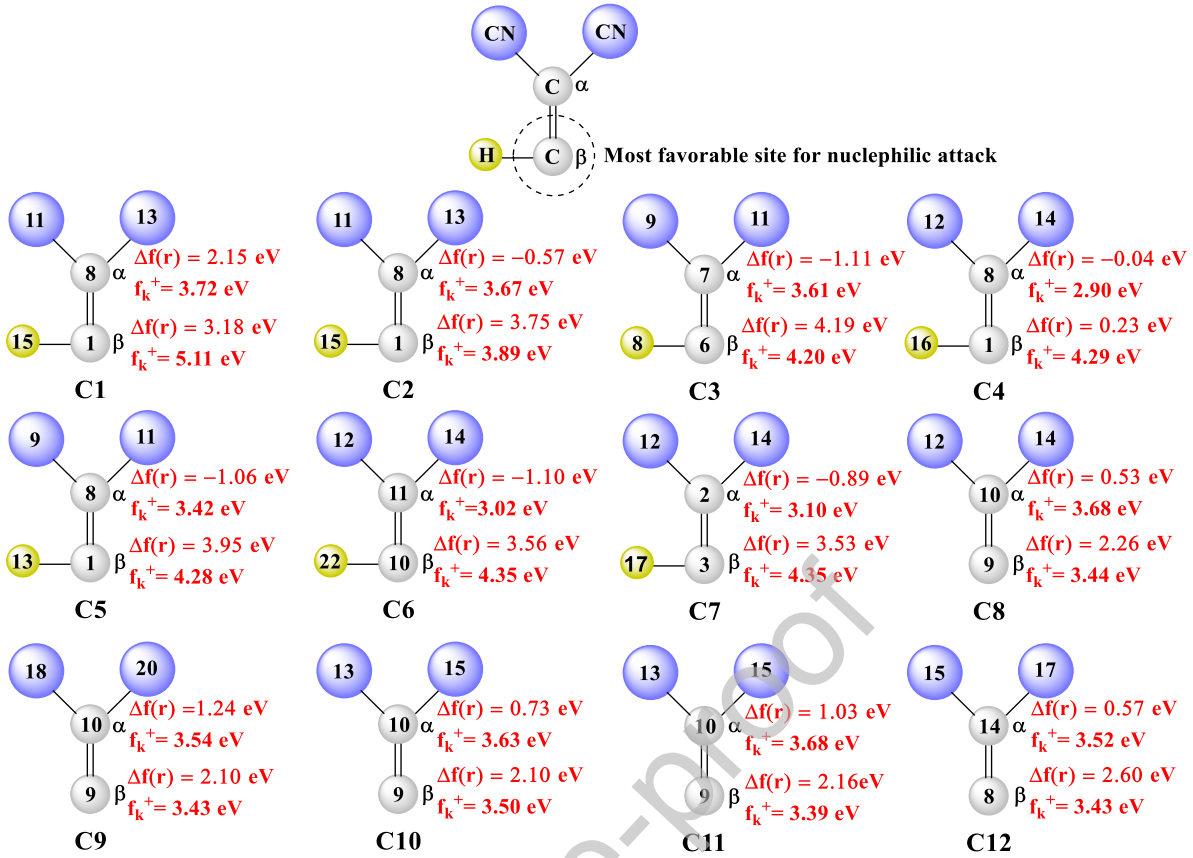

Figure 11. Displayed graphical representation of most favorable site for nucleophilic attack with dual descriptor and Fukui function

Mulliken population analysis (MPA)

The MPA is used to evaluate the Mulliken charge (MC). The evaluations of MC play a dynamic role in the statistical calculation of effects of atomic charge in the exact molecular system that is necessary for the observation of bonding propensities and modification of structural confirmations [51]. In this study, MPA was calculated by DFT/B3LYP/6-31G(d,p) method and presented in the **Supplementary Table 6.** It was found the all the carbon atoms of all compounds C1-C12 were negatively charged except 2C, 8C, 11C and 13C for C1; 2C, 8C, 11C and 13C for C2; 2C, 5C, 11C and 13C for C3; 2C, 5C, 8C, 12C and 14C for C4; 2C, 8C, 9C and 11C for C5; 2C, 3C, 4C, 9C, 12C and 14C for C6;2C, 4C, 6C, 9C, 12C and 14C for C7; 4C, 5C, 8C, 9C, 10C and 12C for C8; 4C, 5C, 8C, 9C, 10C and 12C for C9; 4C, 5C, 8C, 9C, 10C, 13C and 15C for C10; 1C, 4C, 5C, 8C, 9C, 10C, 13C and 15C for C11; 4C, 6C, 7C, 8C, 9C, 14C, 15C and 17C for C12, respectively. These differences were observed due to the bonding with electronegative atoms. The hydrogen atoms had positive charge in the region 0.09-0.34. Nitrogen atom of nitrile groups of all the synthesized alkylidenemalononitrile derivatives (C1-C12) possessed negative charge between 0.450-0.511, respectively. Heterocyclic oxygen of compound C3 and nitrogen of compounds C6, C8, C9, C10 and C11 possessed negative charges -0.436, -0.604, -0.674, -0.706, -0.602 and -0.677, respectively and it was observed that negative charge of heteroatoms increased with the increase of cyclization such as from C3 (-0.436) to C9 (-0.706). Furthermore, it was also found that exocyclic oxygen also carried high negative charge between -0.431-0.565.

Natural population analysis (NPA)

The value of natural charge from NPA denotes statistical stability and defines the electron distribution in the molecular system. The NPA is listed in Supplementary Table 7. The carbon atoms possessed negative charge with the exception of 11C and 13C for C1; 3C, 11C and 13C for C2; 2C, 5C, 9C and 11C for C3; 5C, 12C and 14C for C4; 9C and 11C for C5; 2C, 9C, 12C and 14C for C6; 6C, 9C, 12C and 14C for C7; 4C, 5C, 8C, 9C, 10C, 12C and 14 for C8; 4C, 8C, 12C, 18C and 20C for C9; 4C, 8C, 13C and 15C for C10; 4C, 8C, 13C and 15C for C11; 8C, 9C, 15C and 17C for C12, respectively. These differences were due to attachment of electronegative atoms. All carbon atoms of nitrile group were positively charged between 0.268-0.284 while, nitrogen atoms carried negative charge between -0.237-0.308, respectively. Exocyclic oxygen atoms also possessed negative charge -0.535, -0.533, -0.546, -0.531 and -0.485, respectively for compounds C8-C12. Furthermore, heterocyclic oxygen (-0.430 for C3) and nitrogen (-0.539, -0.634, -0.451, -0.444 and -0.633 for compounds C6, C8, C9, C10 and C11) atoms also carried negative charges.

NBO analysis

NBO study gives maximum information for the evaluation of hybridization, covalence, hydrogen-bonding and Van der Waals interactions along with electron density delocalization from donor (Lewis-type NBO) and acceptor (non-Lewis-type NBO) orbitals [25]. Second-order perturbation theory is utilized to calculate the strength of interaction between Lewis and non-Lewis NBO. For each donor (i) and acceptor (j), the stabilization energy ($E^{(2)}$) related with electron delocalization among donor and acceptor was calculated. High stabilization energy represents strong interaction among donor (i) and acceptor (j) orbitals [25]. The electron density at the conjugated π bonds was (1.64622-1.67852 for C1, 1.62618-1.66606 for C2, 1.74022-1.79581 for C3, 1.57667-1.73786 for C4, 1.60625-1.65897 for C5, 1.61231-1.71992 for C6, 1.62236-1.72251 for C7, 1.63161-1.65724 for C8, 1.63047-1.67581 for C9, 1.63588-1.65938 for C10, 1.63767-1.65801 for C11 and 1.52388-1.70939 for C12) and π* bonds (0.31498–0.43276 for C1, 0.27300–0.46569 for C2, 0.26326-0.34597 for C3, 0.26715-0.44319 for C4,0.27806-0.39711 for C5, 0.28802-0.47344 for C6, 0.33973-0.41917 for C7, 0.33117-0.39311 for C8, 0.31527-0.39339 for C9, 0.32824-0.38727 for C10, 0.36756-0.38788 for C11 and 0.24583-0.43331 for C12) of conjugated ring robust π-electron delocalization under the ring system prominent to a highest stabilization of energy 22.85 for C1, 22.21 for C2, 24.07 for C3, 28.75 for C4, 23.34 for C5, 21.25 for C6, 23.77 for C7, 24.45 for C8, 24.42 for C9, 24.16 for C10, 23.08 for C11 and 20.20 for C12 kcal/mol. Therefore, the donor (i) aptitude of π bonding NBOs are higher with lowest occupancy as compared to σ bonding on the other hand highest occupancies of the π* anti-bonding NBOs indicate their better acceptor (j) aptitude. The alkylidenemalononitrile derivatives (C1-C12) were characterized by the presence of two nitrile groups, which played a major role the in stabilization and reactivity of the molecular system. Hence, a significant resonance in the molecule system was found from the electron donation by nitrogen atom n(1)N (first) and n(1)N (second) to the adjacent σ*(1)C−C bond with the stabilization energy of between 12.81-13.22 kcal/mol depicted in the **Table 10.**

Table 10. Second order perturbation theory analysis of the Fork matrix in the NBO basis for intramolecular interaction for the compounds C1-C12 unit 1

Donor NBO (i)	Occupancy	Acceptor NBO (j)	Occupancy	$(E^2)^a$ (kcal/mol)	E(j)-E(i)^b (a.u.)	F (i,j)^c (a.u.)
C1 (within unit 1)						
σ (1)C11−N12	1.99568	σ* (1)C8−C11	0.03504	6.15	1.53	0.087

n (3)C11−N12	1.95640	π* (2)C1−C8	0.13576	8.92	0.35	0.051
σ (1)C13−N14	1.99555	σ* (1)C8−C13	0.03834	6.18	1.53	0.088
n (3)C13−N14	1.95332	π* (2)C1−C8	0.13576	9.54	0.35	0.053
n(1)N12	1.96920	σ* (1)C8−C11	0.13576	12.94	1.00	0.102
n(1)N14	1.96899	σ* (1)C8−C13	0.03834	13.01	1.00	0.102
		C2 (within unit 1)				
σ (1)C11−N12	1.99569	σ* (1)C8−C11	0.03359	6.18	1.53	0.087
n (3)C11−N12	1.95677	π* (2)C1−C8	0.20078	8.27	0.34	0.049
σ (1)C13−N14	1.99505	σ* (1)C8−C13	0.03905	6.20	1.54	0.088
n (3)C13−N14	1.95377	π* (2)C1−C8	0.20078	8.94	0.35	0.052
n(1)N12	1.96873	σ* (1)C8−C11	0.03359	13.06	1.00	0.102
n(1)N14	1.96810	σ* (1)C8−C13	0.03905	12.96	1.01	0.102
		C3 (within unit 1)				
σ (1)C9−N10	1.99566	σ* (1)C7−C9	0.03310	6.24	1.53	0.088
n (3)C9−N10	1.95830	π* (2)C6−C7	0.25630	8.17	0.34	0.050
σ (1)C11−N12	1.99547	σ* (1)C7−C11	0.03690	6.30	1.54	0.089
n (3)C11−N12	1.95331	π* (2)C6−C7	0.25630	9.09	0.34	0.052
n(1)N10	1.96898	σ* (1)C7−C9	0.03310	12.96	1.01	0.102
n(1)N10	1.96925	σ* (1)C7−C11	0.03690	12.96	1.01	0.102
		C4 (within unit 1)				
σ (1)C12−N13	1.99568	σ* (1)C8−C12	0.03312	6.20	1.54	0.088
n (3)C12−N13	1.96401	π* (2)C1−C8	0.26253	7.46	0.34	0.048
σ (1)C14−N15	1.99510	σ* (1)C8−C14	0.03793	6.23	1.55	0.088
n (3)C14−N15	1.96041	π* (2)C1−C8	0.26253	8.08	0.35	0.050
n(1)N13	1.96880	σ* (1)C8−C12	0.03312	12.90	1.01	0.102
n(1)N15	1.96819	σ* (1)C8−C14	0.03793	12.81	1.02	0.102
		C5 (within unit 1)				
σ (1)C9−N10	1.99572	σ* (1)C8−C9	0.03356	6.16	1.53	0.087
n (3)C9−N10	1.95958	σ* (1)C1−C8	0.20653	8.04	0.34	0.049
σ (1)C11−N12	1.99513	σ* (1)C8−C11	0.03852	6.20	1.54	0.088
n (3)C11−N12	1.95599	π* (2)C1−C8	0.20653	8.73	0.35	0.051
n(1)N10	1.96881	σ* (1)C8−C9	0.03356	12.98	1.01	0.102
n(1)N12	1.96825	σ* (1)C8−C11	0.03852	12.90	1.01	0.102
		C6 (within unit 1)				
σ (1)C12−N13	1.99475	σ* (1)C11−C12	0.03796	6.38	1.55	0.089
n (3)C12−N13	1.96224	σ* (1)C10−C11	0.27038	8.21	0.35	0.051
σ (1)C14−N15	1.99577	σ* (1)C11−C14	0.03279	6.13	1.53	0.087
n (3)C14−N15	1.96515	π* (2)C10−C11	0.27038	7.32	0.34	0.047
n(1)N13	1.96704	σ* (1)C11−C12	0.03796	12.80	1.02	0.102
n(1)N15	1.96850	σ* (1)C11−C14	0.03279	12.94	1.01	0.102
		C7 (within unit 1)				
σ (1)C12−N13	1.99502	σ* (1)C2−C12	0.03815	6.18	1.55	0.088
n (3)C12−N13	1.96015	σ* (1)C2−C3	0.24483	8.12	0.35	0.050
σ (1)C14−N15	1.99567	σ* (1)C2−C14	0.03325	6.22	1.53	0.088
n (3)C14−N15	1.96237	π* (2)C2−C3	0.24483	7.68	0.34	0.048
n(1)N13	1.96783	σ* (1)C2−C12	0.03815	12.80	1.02	0.102
n(1)N15	1.96880	σ* (1)C2−C14	0.03325	12.96	1.01	0.102
		C8 (within unit 1)				
σ (1)C12−N13	1.99526	σ* (1)C10−C12	0.03467	6.12	1.54	0.087
π (2)C12−N13	1.98174	π* (2)C9−C10	0.24355	8.92	0.35	0.053
σ (1)C14−N15	1.99546	σ* (1)C10−C14	0.03593	6.26	1.53	0.088
π (2)C14−N15	1.98181	π* (2)C9−C10	0.24355	9.87	0.34	0.054
n(1)N13	1.96793	σ* (1)C10−C12	0.03467	13.00	1.01	0.102
n(1)N15	1.96884	σ* (1)C10−C14	0.03593	13.18	1.00	0.103
		C9 (within unit 1)				
σ (1)C18−N19	1.99525	σ* (1)C10−C18	0.03452	6.13	1.54	0.087
π (2)C18−N19	1.98165	π* (2)C9−C10	0.24513	8.87	0.36	0.05
σ (1)C20−N21	1.99545	σ* (1)C10−C20	0.03589	6.25	1.53	0.088
π (2)C20−N21	1.98181	π* (2)C9−C10	0.24513	9.82	0.34	0.054
n(1)N19	1.96791	σ* (1)C10−C18	0.03452	12.99	1.01	0.102
n(1)N21	1.96880	σ* (1)C10−C20	0.03589	13.18	1.00	0.103
		C10 (within unit 1)				
σ (1)C13−N14	1.99527	σ* (1)C10−C13	0.03461	6.11	1.54	0.087
π (2)C13−N14	1.98177	π* (2)C9−C10	0.24212	8.87	0.36	0.053
σ (1)C15−N16	1.99546	σ* (1)C10−C15	0.03591	6.25	1.53	0.088
π (2)C15−N16	1.98184	π* (2)C9−C10	0.24212	9.82	0.34	0.054
n(1)N14	1.96794	σ* (1)C10−C13	0.03461	12.99	1.01	0.102
n(1)N16	1.96884	σ* (1)C10−C15	0.03591	13.17	1.00	0.103
		C11 (within unit 1)				
σ (1)C13−N14	1.99545	σ* (1)C10−C13	0.03599	6.28	1.53	0.088
π (2)C13−N14	1.98178	π* (2)C9−C10	0.23778	10.10	0.34	0.055
σ (1)C15−N16	1.99522	σ* (1)C10−C15	0.03473	6.14	1.54	0.087
π (2)C15−N16	1.98155	π* (2)C9−C10	0.23778	9.16	0.35	0.053
n(1)N14	1.96885	σ* (1)C10−C13	0.03599	13.22	1.00	0.103
n(1)N16	1.96786	σ* (1)C10−C15	0.03473	13.06	1.01	0.103

C12 (within unit 1)						
σ (1)C15−N16	1.99548	σ* (1)C14−C15	0.03685	6.18	1.53	0.087
π (3)C15−N16	1.94090	π* (2)C8−C14	0.22566	9.77	0.34	0.054
σ (1)C17−N18	1.99528	σ* (1)C14−C17	0.03503	6.07	1.54	0.087
π (3)C17−N18	1.94855	π* (2)C8−C14	0.22566	8.84	0.36	0.052
n(1)N16	1.96882	σ* (1)C14−C15	0.03685	13.15	1.00	0.103
n(1)N18	1.96782	σ* (1)C14−C17	0.03503	12.97	1.01	0.102

In-silico bioactivity evaluation

Molecular Docking (AutoDock)

Crystal structures of receptors were downloaded from the Protein Data Bank (www.rcsb.org). For the receptor structure cleaning, hydrogen atoms were added, minimally used residue structures were deleted, and every partial side chain was replaced. Additionally, AutoDock Tools was used to eliminate crystal water. Gasteiger charges were added to each atom and non-polar hydrogen atoms were merged to the protein structure [54]. The distance between donor and acceptor atoms that forms a hydrogen bond was defined as 1.9 Å with a receiving of 0.5 Å and the acceptor hydrogen donor angle was not less than 120°. The grid box was set with dimensions of 20×20×20 $Å^3$ and grid box was centered on 50.461, 35.357 and 96.121 for HCK_HUMAN and 216.497, 147.531, 156.502 for RNR_HUMAN formed around the binding site of synthesized compounds on the receptor. Finally, grid energy calculations were carried out. For the binding energy calculation, default parameters were used, and 100 docked conformations were generated for each synthesized compound. Complete docking involved 2.5 million energy assessments. Docked ligand conformations were studied in terms of energy, hydrogen bonding, hydrophobic interaction and dissociation constant (K_d) between the ligand and receptor (**Table 11** and Supplementary Table 2).

Comprehensive evaluations of the ligand-receptor interactions were done, and final coordinates of the ligand and receptor were saved as .pdb files. For display of the ligand-receptor binding site, BDS visualizer was used. Compound C12 was most active with the calculated binding energy (BE) of -6.1 kcal/mol and K_d 34.04 µM with respect to HCK_HUMAN and BE of -6.98 kcal/mol and K_d of 7.64 µM with respect to RNR_HUMAN. Doxorubicin HCl and tetracycline were used as reference drugs. The binding interactions of these compounds have been displayed as **Supplementary Figure 1.**

Table 11. Average AutoDock energy values obtained in docking of compounds C1-C12

	AutoDock findings						
					Interacting Amino acids		
Receptor	**Est. binding energy (kcal/mol)**	**Est. dissociation constant (K_d)**	**Ligand Efficiency**	**Intermol Energy**	**Van der Waals force**	**Hydrogen Bonds**	**π and other interactions**
5ZJ6	-5.52	123.55	-0.36	-5.57	THR338, GLU339, GLY344, ASP404	ILE336	LEU273, VAL281, ALA293, LYS295, MET341, LEU393, ALA403, LEU407
6AUI	-5.33	205.84	-0.35	-5.39	GLU11, ARG12, ASP57	ARG12	VAL13, MET14, LYS17, ILE18, ARG21, LEU56, ALA60

Molecular Docking (iGEMDOCK)

The docking results **(Table 17)** revealed that compound C12 exhibited the lowest docking energies with respect to HCK_HUMAN (-102.619 kcal/mole) and RNR_HUMAN (-95.483 kcal/mole). In some cases, common interacting amino acids residues were obtained in both the docking programs. Likewise, the average binding energy of synthesized compounds with

respect to HCK_HUMAN was -83.454 with a SD of 8.836 and variance of 78.078. Likewise, the average binding energy of synthesized compounds with respect to RNR_HUMAN was -79.807 with a SD and variance of 7.925 and 62.812 respectively as depicted in **Table 12** and **Figure 12** (Supplementary Table 3 and Figure 2).

Table 12. Average iGEMDOCK energy values obtained in docking of compounds C1-C12

	iGEMDOCK findings						
Receptor	**Est. total energy**	**Van der Waals energy**	**Hydrogen Bond energy**	**Electrostatic potential energy**	**Interacting Amino acids**		
					Van der Waals force	**Hydrogen Bonds**	**π and other interactions**
5ZJ6	-83.45	-72.19	-11.27	0	ALA293, MET314, VAL323, LEU393, ILE402, ASP404	THR338	VAL281, LYS295, ILE336, ALA403, PHE405, LEU407
6AUI	-78.06	-62.66	-15.40	0	GLU11, ARG12, VAL13, MET14, LYS17, ILE22, LEU56, ALA60	ARG6, THR53	ILE18, ARG21, VAL43,

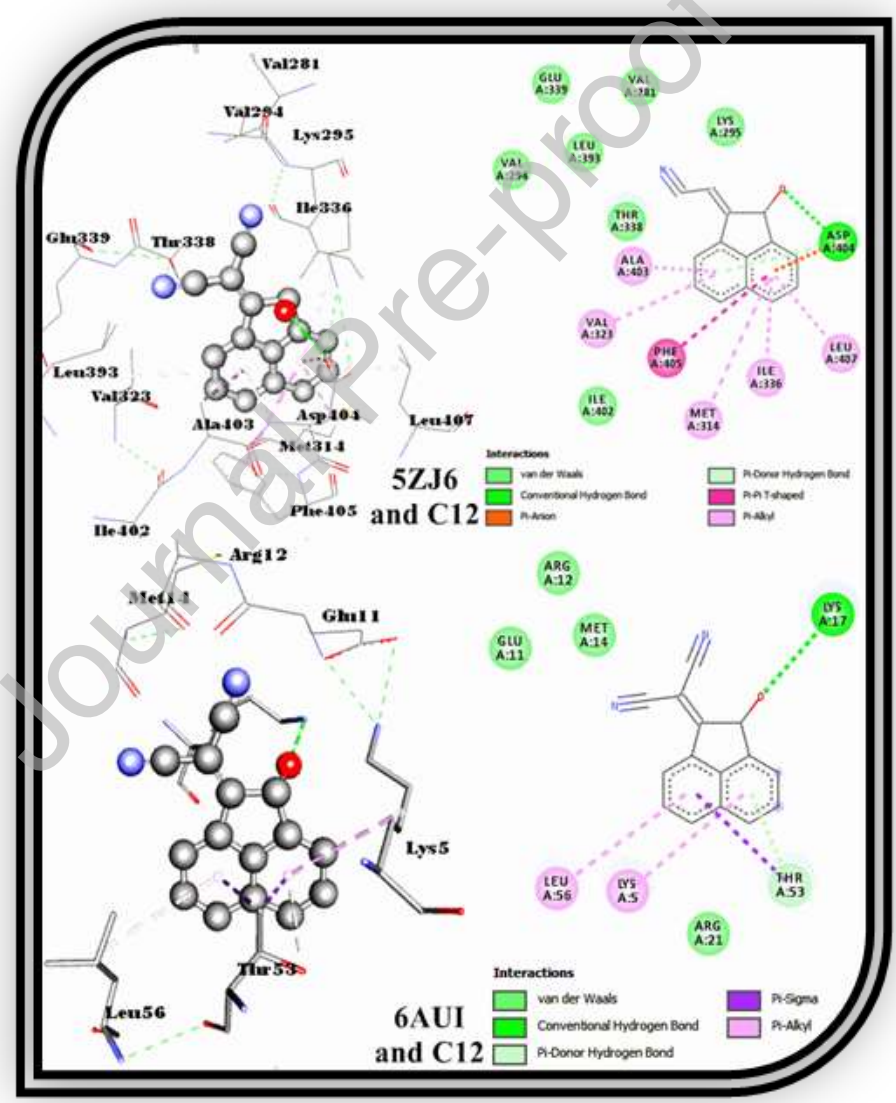

Figure 12. Two- and three-dimensional (2D and 3D) representation of compound C12 and target proteins (5ZJ6 and 6AUI) obtained from iGEMDOCK

Metabolic transformations prediction

MetaPrint2D identifies the metabolic sites within the molecule and gives an idea about the how a subjected molecule will be metabolized in the body. Different colors indicate altered levels of metabolic sites as shown in **Table 1.** The NOR is obtained from the recorded database. A higher NOR value indicates a regularly described site of metabolism.

Molecular parameters

All malononitrile derivatives obeyed Lipinski's rule with a maximum of one violation. Interestingly, none of the synthesized compounds were found to violate leadlikeness rule. Therefore, malononitrile derivatives were found to possess properties so as to make them suitable for development into drugs [12] (Supplementary Table 14).

ADMET prediction

All the synthesized compounds showed good BBB penetrability as well as HIA and Caco2 cell permeability [45]. With the exception of C4, none of them showed carcinogenicity. In case of toxicity assessment, with the exception of C1, C2, C8 and C11-C13 all the synthesized malononitrile derivatives were found to be nontoxic. They also displayed excellent LD_{50} values in rats (Supplementary Table 15).

Toxicity Potential

All the compounds were found to be nontoxic with no expected tumorigenicity, irritant effect or adverse effect on the reproductive system. Principle Component Analysis (PCA) was also implemented on drug like properties *viz.* cLogP, cLogS and druglikeness (DL) with the help of linear correlation between the variables (Supplementary Table 16) **(Figure 13)**. PCA analysis represents that synthesized malononitrile derivatives displayed moderate DL except compound 2, 9 and 12.

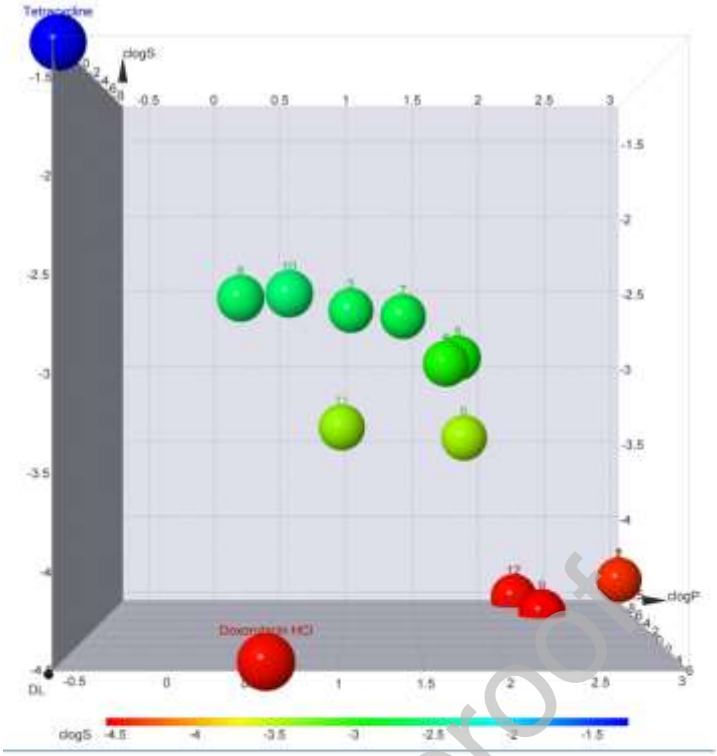

Correlation coefficient or r (Spearman (correlation of ranks)

		1	2	3	4	5	6
clogP	1		-0.631	-0.549	0.991	0.294	0.345
clogS	2	-0.631		0.037	-0.640	-0.714	0.063
DL	3	-0.549	0.037		-0.536	0.475	-0.111
pc1	4	0.991	-0.640	-0.536		0.319	0.310
pc2	5	0.294	-0.714	0.475	0.319		0.098
pc3	6	0.345	0.063	-0.111	0.310	0.098	

Figure 13. PCA (Scatter plot) of toxicological parameters and drug like properties (cLogP, cLogS, DL) of the synthesized compounds C1-C12 and standard drugs doxorubicin HCl (13) and tetracycline (14), along with Spearman correlation ranks.

Bioactivity score prediction

The bioactivity scores of all the synthesized compounds are depicted in **Table 8.** The predicted values were between -0.34 and -1.66 with respect to GPCR; -0.41 and -125 with respect to ICM; -0.07 and -1.94 with respect to KI, -0.66 and -1.94 with respect to NRL; -0.16 and -2.19 with respect to PI as well as -0.12 and -1.36 with respect to EI. Most of the compounds had bioactivity scores between -5.0 and 0.0 and were predicted to be moderately active. PCA analysis was also done to assess how close are the obtained bioactivity scores of the synthesized compounds with the standard drugs (Supplementary Table 17). PCA investigation was displayed moderate druglikeness of synthesized malononitrile derivative as compared to standard drugs (Figure 14). The consequences of the current study projected that

most of the explored synthesized compounds are biologically active and would show the physiological actions by interacting with various biological targets.

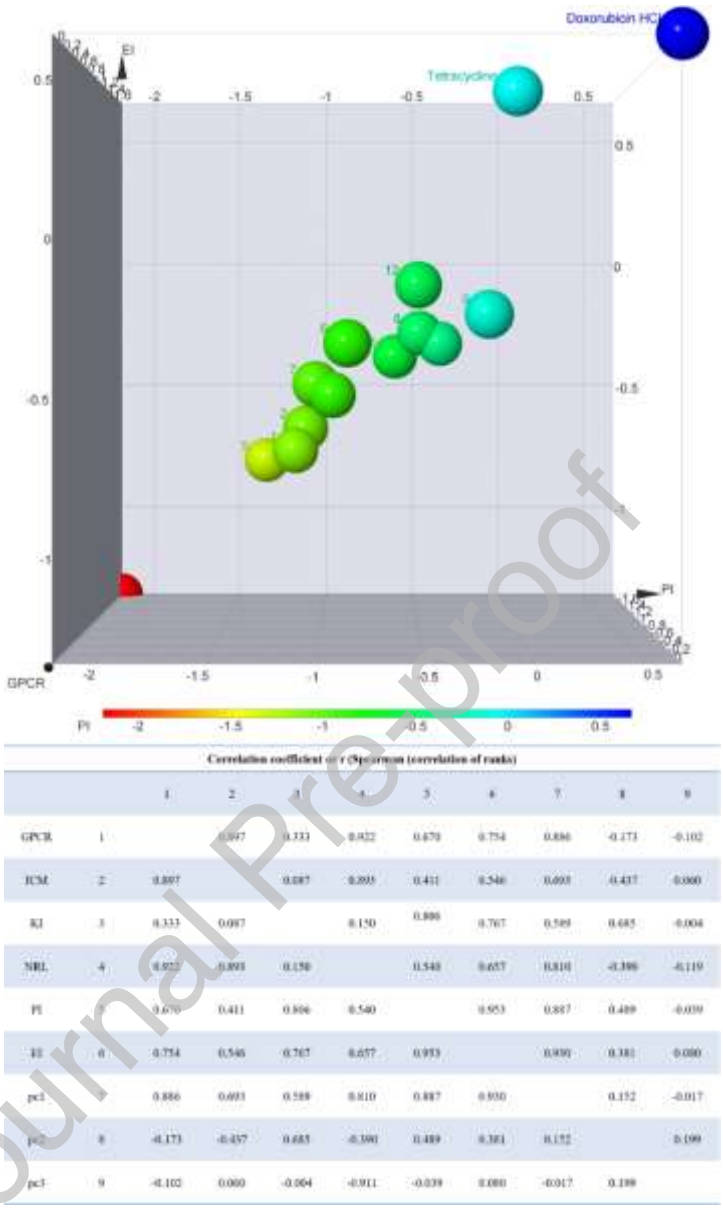

		1	2	3	4	5	6	7	8	9
GPCR	1		0.897	0.333	0.922	0.670	0.754	0.886	-0.173	-0.102
ICM	2	0.897		0.087	0.893	0.411	0.546	0.693	-0.457	0.000
KI	3	0.333	0.087		0.150	0.806	0.767	0.589	0.685	-0.004
NRL	4	0.922	0.893	0.150		0.540	0.657	0.810	-0.390	-0.119
PI	5	0.670	0.411	0.806	0.540		0.953	0.887	0.489	-0.039
EI	6	0.754	0.546	0.767	0.657	0.953		0.930	0.381	0.080
pc1	7	0.886	0.693	0.589	0.810	0.887	0.930		0.152	-0.017
pc2	8	-0.173	-0.457	0.685	-0.390	0.489	0.381	0.152		0.199
pc3	9	-0.102	0.000	-0.004	-0.911	-0.039	0.080	-0.017	0.199	

Figure 14. PCA (Scatter plot) of bioactivity scores of the synthesized compounds C1-C12 and standard drugs Doxorubicin HCl (13) and Tetracycline (14), along with Spearman correlation ranks.

Biological screening

Anticancer evaluation

Anticancer activity of the synthesized compounds was tested against MDA-MB-231 cell line using MTT assay in the concentration range 20-100 µM. Compound 11 was found to be the most active with an IC_{50} of 20 µM followed by compound 9 with an IC_{50} around 50 µM. The anticancer activity of the synthesized compounds decreased in the following order:

11>9>12>10>1>7>8>4>6>3>2>5. **Figure 15** summarizes the dose dependent effect of compounds C1-C12 on the viability of MDA cells.

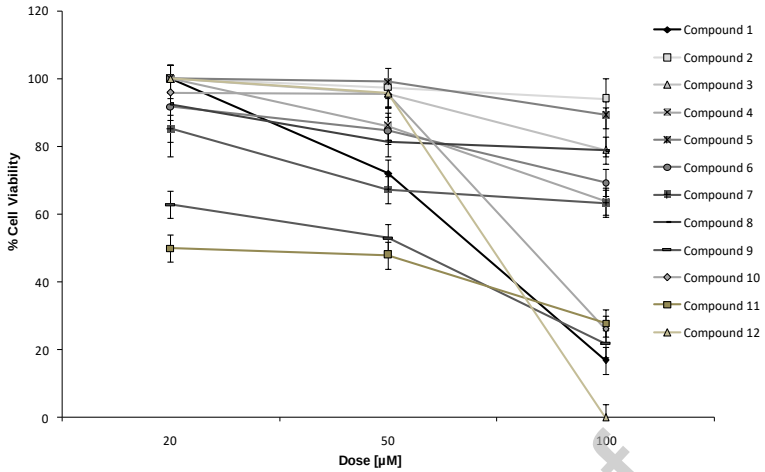

Figure 15. Dose response curves of synthesized compounds C1-C12 on viability of MDA cells *in vitro* using MTT assay. Final concentration of DMSO in each well did not exceed 0.5% (v/v). Results are expressed as mean ± SD of treatments done in triplicates

Antibacterial evaluation

Compounds C1-C12 were evaluated for their potential antibacterial activity against two species of bacteria *viz. Staphylococcus aureus* and *Escherichia coli* using disc diffusion method in the range 2-20 mg. While compounds C1, C8, C9, C11 and C12 exhibited good activity against *S. aureus*, compounds C2-C7 as well as C10, did not exhibit any significant activity against *S. aureus*. All compounds exhibited little to no activity against the gram-negative bacterium *E. coli*. Compound 1 exhibited activity against *S. aureus* from 6 mg onwards (Figure 17 (1) while it was found to be active against *E. coli* from 16 mg onwards (Figure 16 (1). Compound C8 was highly active against *S. aureus* (MIC 10.0 mg/mL) whereas it showed slight activity against *E. coli* (MIC 10.0 mg/mL). Compound 9 was active against *S. aureus* (MIC 2.0 mg/mL) whereas it showed no activity against *E. coli*. Compound 10 was not active against either *S. aureus* or *E. coli*. Compound C11 was found to be highly active against *S. aureus* (MIC 6.0 mg/mL) and it showed a little activity against *E. coli*, more than compound 8 (MIC 10.0 mg/mL). Interestingly, compound C11 was also found to possess the strongest cytotoxic activity against MDA cells as compared to other compounds **(Figure 16-17 and Table 13).** Of all the compounds tested for antibacterial activity, compound C12 was found to be the most active (MIC 2.0 mg/mL) against *S. aureus*. Thus, compounds C9, C11 and C12 have the potential to emerge as potential anticancer and antibacterial agents, if studied and tested further for their anticancer and antibacterial activity *in vitro* as well as *in vivo*.

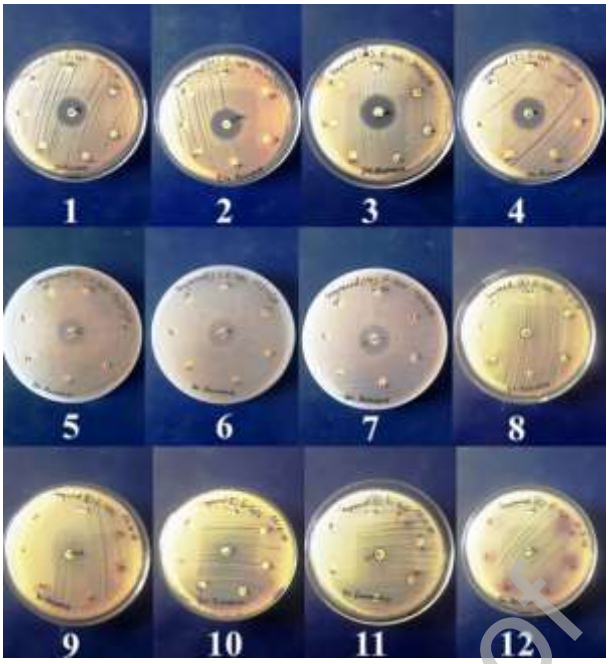

Figure 16. Antibacterial activity of compounds C1-C12 against *E. coli* using disc diffusion method

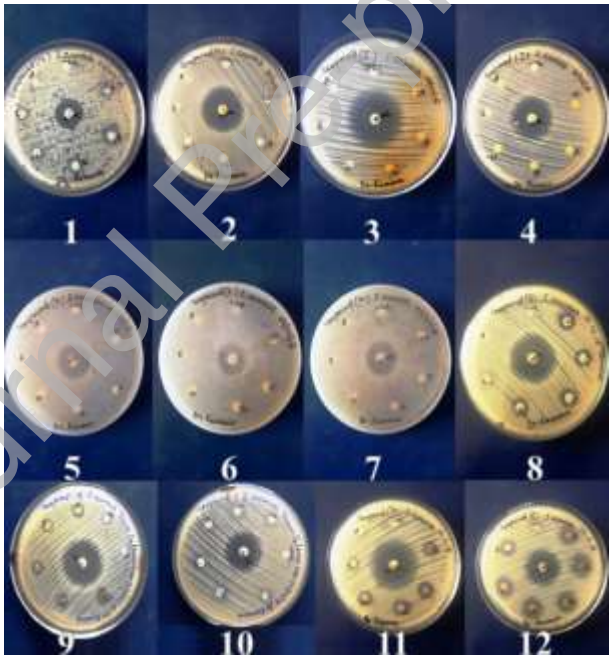

Figure 17. Antibacterial activity of compounds C1-C12 against *S. aureus* using disc diffusion method

Table 13. Comparison of minimum inhibitory concentration (MIC) values in mg/mL of Compounds C1-C12 and standard antibiotic tetracycline against *E. coli* and *S. aureus*

Entry	*E. coli*				*S. aureus*			
	Tetracycline (30 mg/mL)	**DMSO (100%)**	**Compound Dose (mg/mL)**	**Ring diameter (cm)**	**Tetracycline (30 mg/mL)**	**DMSO (100%)**	**Compound Dose (mg/mL)**	**Ring diameter (cm)**
C1	2.0	ND	2	nil	2.0	ND	2	nil
			6	nil			6	0.7
			10	nil			10	0.8
			16	0.6			16	0.9
			18	0.7			18	1.1

			20	0.8			20	0.8
C2	2.0	ND	2	nil	2.8	ND	2	nil
			6	nil			6	nil
			10	nil			10	nil
			16	nil			16	nil
			18	nil			18	nil
			20	nil			20	nil
C3	2.3	ND	2	nil	3.0	ND	2	nil
			6	nil			6	nil
			10	nil			10	nil
			16	nil			16	nil
			18	nil			18	nil
			20	nil			20	nil
C4	2.0	ND	2	nil	2.5	ND	2	nil
			6	nil			6	nil
			10	nil			10	nil
			16	nil			16	nil
			18	nil			18	nil
			20	nil			20	nil
C5	2.0	ND	2	nil	2.3	ND	2	nil
			6	nil			6	nil
			10	nil			10	nil
			16	nil			16	nil
			18	nil			18	nil
			20	nil			20	nil
C6	2.0	ND	2	nil	2.0	ND	2	nil
			6	nil			6	nil
			10	nil			10	nil
			16	nil			16	nil
			18	nil			18	nil
			20	nil			20	nil
C7	2.0	ND	2	nil	2.1	ND	2	nil
			6	nil			6	nil
			10	nil			10	nil
			16	nil			16	nil
			18	nil			18	nil
			20	nil			20	nil
C8	1.0	ND	2	nil	3.0	ND	2	nil
			6	nil			6	nil
			10	0.4			10	0.9
			16	0.4			16	1.2
			18	0.5			18	1.3
			20	0.5			20	1.4
C9	0.8	ND	2	nil	2.8	ND	2	0.6
			6	nil			6	0.8
			10	nil			10	0.7
			16	nil			16	0.8
			18	nil			18	0.8
			20	nil			20	1.0
C10	0.8	ND	2	nil	2.5	ND	2	nil
			6	nil			6	nil
			10	nil			10	nil
			16	nil			16	nil
			18	nil			18	nil
			20	nil			20	nil
C11	0.9	ND	2	nil	3.5	ND	2	nil
			6	nil			6	0.8
			10	0.7			10	0.9
			16	0.8			16	1.0
			18	0.8			18	1.2
			20	0.9			20	1.2
C12	0.9	ND	2	nil	2.5	ND	2	1.3
			6	nil			6	1.5
			10	nil			10	1.7
			16	nil			16	1.8
			18	nil			18	2.0
			20	nil			20	1.9

ND= Not detected

Biological evaluation observations indicated that compounds C8, C9, C11 and C12 have the potential to emerge as potential anticancer and antibacterial agents. It is clear from the results that the structure of the compounds played an important role in determining the biological activity of the synthesized compounds. It was found that the 2-(2-oxo-indolin-3-ylidene) malononitrile derivatives (compounds C8-C12) exhibited better biological activity than 2-benzylidene malononitrile derivatives due to a difference in the structure and due to the presence of an extra ring in the 2-(2-oxo-indolin-3-ylidene) malononitrile derivatives which might have played a role in enhancing the biological activity spectrum of compounds C8-C12 as compared to compounds C1-C7.

Structure Activity Relationships (SAR)

Structure activity relationships were also validated from the docking results and DFT calculations. E_{HOMO}, E_{LUMO} and E_{GAP} are the most significant parameters for the identification of physiochemical properties, chemical reactivity and biological behavior of chemical entities. E_{HOMO} and E_{LUMO} govern the electrophilic and nucleophilic attacks while electron-donating proficiency of the molecule system is evaluated by the decrease in the value of E_{GAP}. Initial investigations showed that compounds C1-C7 had only 1-4 van der Waals (VDW) interactions with some common amino acid residues such as THR338 and ASP404 in the binding pocket of HCK_HUMAN (5ZJ6) and GLU11, ARG12, MET14, THR53 and ASP57 with respect to RNR_HUMAN (6AUI). On the other hand, compounds 8-12 had 3-8 such interactions with LEU274, VAL294, LYS295, THR338, MET341, GLY344 and ASP404 in the binding pocket of HCK_HUMAN and LYS5, GLU11, ARG12, VAL13, THR53, LEU56 and ASP57 with respect to RNR_HUMAN. The value of E_{GAP} was between 3.62-4.81eV for compounds C1-C7 and 2.90-3.29 eV for compounds C8-C12. Therefore, the presence of additional aromatic ring in the ligand molecule may have caused better binding due to the increase in the VDW and hydrophobic interactions with the receptor proteins.

Compound C11 (5-bromoisatin) possessed excellent antibacterial as well as anticancer activity as compared to other compounds because of the substitution of bromine atom at the fifth position of the phenyl ring. Bromine may have activated the isatin ring system and from the E_{GAP} value (2.94eV), it was found that C11 had good electron donation capacity. The VDW and H-bond forming tendency of 5-bromoisatin was higher; forming 5-8 VDW interactions, 1-4 H-bonds and bromine itself was observed to form pi-alkyl bond. After derivatization of isatin, hydrogen of N-H position was replaced with methyl and phenyl groups. When the H atom of isatin was replaced by methyl group then the antibacterial activity spectrum of isatin decreased and the value of E_{GAP} (3.04 eV) increased. On the other hand, when it was replaced by phenyl ring, then a marginal loss in the activity was observed and the value of E_{GAP} (2.90 eV) was nearly same as C11. After the analysis of docking poses, it was found that isatin has more probability to form H-bonding maximally at N-H position. When hydrogen atom of the N-H group was replaced with the methyl group, then isatin lost its tendency to form H-bond with N-H group and methyl was found to be involved in the alkyl interaction. Replacement of hydrogen with phenyl ring further decreased the H-bond forming tendency but VDW and alkyl interactions increased. Analysis of E_{GAP} values also support the electron donation capacity and the biological activity. Compounds C9, C10 and

C11 possessed E_{GAP} values of 3.04, 2.90 and 2.94 eV, respectively. Compounds C10 and C11 had nearly same values of E_{GAP} but compound C11 showed superior biological activity due to the presence of NH group. However, the flip side was that the extra ring also afforded toxic side effects to compounds C8, C11, C12 and C13, as predicted by admetSAR and to compound C12, as predicted by OSIRIS Data Warrior.

Conclusion

An eco-friendly and efficient, grinding induced Knoevenagel condensation of aldehyde/ketone and malononitrile for the synthesis of malononitrile scaffolds in PEG-400/water solvent has been proposed. The title malononitrile scaffolds were obtained in a short time in relatively high yield. The chemical structures of all the alkylidenemalononitrile derivatives C1-C12 were optimized through DFT-B3LYP method and 6-311G(d,p) level. The predicted geometrical parameters of the synthesized compounds agreed well with the experimental findings. The alkylidenemalononitrile derivatives C1-C12 were shown to possess superior non-linear optical properties than urea and compounds C3 and C7 are highly recommended to act as NLO candidates as they were found to possess superior NLO properties than urea and para-nitro aniline making them suitable for photonic-communication instruments. The synthesized derivatives were also evaluated for their prospective anticancer and antibacterial activity. Compounds C9, C11 and C12 were found to exhibit good antibacterial and anticancer activities. Many of the synthesized derivatives were found to possess remarkable ADMET properties and druglikeness. Molecular docking studies revealed good interaction between the derivatives and target receptor proteins. The obtained results have established the utility of synthesized malononitrile derivatives as potential anticancer, antibacterial drug candidates as well as potential NLO candidates if studied further *in vitro* and *in vivo*.

Acknowledgements

The authors wish to extend their thanks and appreciation to Mr. Mohsin Ali Khan, Chancellor, Era's University, Lucknow, India, for providing the necessary facilities, support and co-operation for carrying out the biological activity evaluation studies. The authors are also thankful to Dr. Syed Mohd. Danish Rizvi for helping in data analysis. The authors also wish to thank the Bioinformatics Resources & Applications Facility at Centre for Development of Advanced Computing, India, and R&D wing of Integral University, Lucknow, India, for the facilities to carry out the research work.

CREDIT AUTHOR STATEMENT

All persons who meet authorship criteria are listed as authors and all authors certify that they have participated sufficiently in the work to take public responsibility for the content, including participation in the concept, design, analysis, writing or revision of the manuscript. Below are the contribution details of the authors as listed in the paper-

Dr. Iqbal Azad- Conceptualized the study, experimental work, analysis and interpretation of characterization data and drafting the manuscript.

Dr. Tahmeena Khan- Characterization, manuscript preparation, revision and editing.

Dr. Rumana Ahmad- Biological activity evaluation

Dr. Azhar Kamal- Biological activity evaluation

Dr. Abdul Rahman Khan- Proof reading the manuscript

Dr. Malik Nasibullah- Supervision of the study and manuscript proof reading.

Declaration of interests

☒ The authors declare that they have no known competing financial interests or personal relationships that could have appeared to influence the work reported in this paper.

☐The authors declare the following financial interests/personal relationships which may be considered as potential competing interests:

References

[1] J. Huang, J. Zhou, S. Song, H. Song, Z. Chen, W. Yi, A new and efficient ZnCl2-catalyzed synthesis and biological evaluation of novel 2-amino-3,5-dicyano-4-aryl-6-aryl-aminopyridines as potent antibacterial agents against Helicobacter pylori (HP), Tetrahedron. 71 (2015) 8628–8636. doi:10.1016/J.TET.2015.09.018.

[2] W.S. Shehab, A.A. Ghoneim, Synthesis and biological activities of some fused pyran derivatives, Arab. J. Chem. 9 (2016) S966–S970. doi:10.1016/J.ARABJC.2011.10.008.

[3] Geoffrey Wells, and Angela Seaton, M.F.G. Stevens, Structural Studies on Bioactive Compounds. 32.1 Oxidation of Tyrphostin Protein Tyrosine Kinase Inhibitors with Hypervalent Iodine Reagents, J. Med. Chem. 43 (2000) 1550-1562. doi:10.1021/JM990947F.

[4] H. Wang, C. Wang, Y. Yang, M. Zhao, Y. Wang, H3 PW12O40 /mpg-C3N4 as an efficient and reusable bifunctional catalyst in one-pot oxidation–Knoevenagel condensation tandem reaction, Catal. Sci. Technol. 7 (2017) 405–417. doi:10.1039/C6CY01669C.

[5] F. Safari, H. Hosseini, M. Bayat, A. Ranjbar, Synthesis and evaluation of antimicrobial activity, cytotoxic and pro-apoptotic effects of novel spiro-4 H -pyran derivatives, RSC Adv. 9 (2019) 24843–24851. doi:10.1039/c9ra03196k.

[6] M.H. Ahmed, M.A. El-Hashash, M.I. Marzouk, A.M. El-Naggar, Design, Synthesis, and Biological Evaluation of Novel Pyrazole, Oxazole, and Pyridine Derivatives as Potential Anticancer Agents Using Mixed Chalcone, J. Heterocycl. Chem. 56 (2019) 114–123. doi:10.1002/jhet.3380.

[7] A. Priyadharshini, S. Kalainathan, Bulk crystal growth, spectral, optical, thermal, electrical and third-order NLO properties of benzylidene malononitrile derivative single crystal: a promising material for nonlinear optical device applications, J. Mater. Sci. Mater. Electron. 29 (2018) 2698–2708. doi:10.1007/s10854-017-8196-4.

[8] A.P. Dhondge, J.Y. Chen, T. Lin, F.M. Yen, K.W. Li, H.C. Hsieh, M.Y. Kuo, Di-2-(2-oxindolin-3-ylidene)malononitrile Derivatives for N-Type Air-Stable Organic Field-Effect Transistors, Org. Lett. 20 (2018) 40–43. doi:10.1021/acs.orglett.7b03284.

[9] E. Catal, E. Keles, N. Seferoglu, S. Achelle, A. Barsella, F. Robin Le Guen, Z. Seferoglu, Triphenylamine-based allylidenemalononitrile chromophores: Synthesis, and photophysical and second-order nonlinear optical properties, New J. Chem. 42 (2018) 15052–15060. doi:10.1039/c8nj02794c.

[10] D. Zych, A. Slodek, Acceptor-π-Acceptor-Acceptor/Donor systems containing dicyanovinyl acceptor group with substituted 1,2,3-triazole motif – synthesis, photophysical and theoretical studies, J. Mol. Struct. 1204 (2020) 127488. doi:10.1016/j.molstruc.2019.127488.

[11] I.R. Shaikh, Organocatalysis: Key Trends in Green Synthetic Chemistry, Challenges, Scope towards Heterogenization, and Importance from Research and Industrial Point of View, J. Catal. 2014 (2014) 1–35. doi:10.1155/2014/402860.

[12] I. Azad, R. Ahmad, T. Khan, M. Saquib, F. Hassan, Y. Akhter, A.R. Khan, M. Nasibullah, Phenanthridine derivatives as promising new anticancer agents: Synthesis, biological evaluation and binding studies, Future Med. Chem. 12 (2020) 709–739. doi:10.4155/fmc-2019-0016.

[13] S. Wang, Z. Ren, W. Cao, W. Tong, The Knoevenagel Condensation of Aromatic Aldehydes with Malononitrile or Ethyl Cyanoacetate in the Presence of ctmab in Water, Synth. Commun. 31 (2001) 673–677. doi:10.1081/SCC-100103255.

[14] Z. Ren, W. Cao, W. Tong, The Knoevenagel Condensation Reaction of Aromatic Aldehydes with Malononitrile by Grinding in the Absence of Solvents and Catalysts, Synth. Commun. 32 (2002) 3475–3479. doi:10.1081/SCC-120014780.

[15] D. V. Demchuk, M.N. Elinson, G.I. Nikishin, 'On water' Knoevenagel condensation of isatins with malononitrile, Mendeleev Commun. 21 (2011) 224–225. doi:10.1016/J.MENCOM.2011.07.018.

[16] P. Grenni, V. Ancona, A.B. Caracciolo, Ecological effects of antibiotics on natural ecosystems: A review, Microchem. J. 136 (2017) 25–39. doi:10.1016/j.microc.2017.02.006.

[17] N. Moshina, S. Sebuodegard, C.I. Lee, L.A. Akslen, K.M. Tsuruda, J.G. Elmore, S. Hofvind, Automated Volumetric Analysis of Mammographic Density in a Screening Setting: Worse Outcomes for Women with Dense Breasts, Radiology. 288 (2018) 343-352. doi:10.1148/radiol.2018172972.

[18] E. Torrents, Ribonucleotide reductases: essential enzymes for bacterial life., Front. Cell. Infect. Microbiol. 4 (2014) 52. doi:10.3389/fcimb.2014.00052.

[19] M.A. Khajah, I. Almohri, P.M. Mathew, Y.A. Luqmani, Extracellular Alkaline pH Leads to Increased Metastatic Potential of Estrogen Receptor Silenced Endocrine Resistant Breast Cancer Cells, PLoS One. 8 (2013) e76327. doi:10.1371/journal.pone.0076327.

[20] T. Mosmann, Rapid colorimetric assay for cellular growth and survival: application to proliferation and cytotoxicity assays., J. Immunol. Methods. 65 (1983) 55–63. doi:10.1016/0022-1759(83)90303-4

[21] M. Balouiri, M. Sadiki, S.K. Ibnsouda, Methods for in vitro evaluating antimicrobial activity: A review, J. Pharm. Anal. 6 (2016) 71–79. doi:10.1016/J.JPHA.2015.11.005.

[22] A.A. Mostafa, A.A. Al-Askar, K.S. Almaary, T.M. Dawoud, E.N. Sholkamy, M.M. Bakri, Antimicrobial activity of some plant extracts against bacterial strains causing food poisoning diseases, Saudi J. Biol. Sci. 25 (2018) 361–366. doi:10.1016/J.SJBS.2017.02.004.

[23] M. J. Frisch, G. W. Trucks, H. B. Schlegel, G. E. Scuseria, M. A. Robb, et al., Gaussian 09, Revision A.02, Gaussian, Inc., Wallingford CT, 2009.

[24] M. Szafran, A. Komasa, E. Bartoszak-Adamska, Crystal and molecular structure of 4-carboxypiperidinium chloride (4-piperidinecarboxylic acid hydrochloride), J. Mol. Struct. 827 (2007) 101–107. doi:10.1016/j.molstruc.2006.05.012.

[25] I. Azad, Y. Akhter, T. Khan, M.I. Azad, S. Chandra, P. Singh, D. Kumar, M. Nasibullah, Synthesis, quantum chemical study, AIM simulation, in silico ADMET profile analysis, molecular docking and antioxidant activity assessment of aminofuran derivatives, J. Mol. Struct. 1203 (2020) 127285. doi:10.1016/j.molstruc.2019.127285.

[26] E.D. Glendening, C.R. Landis, F. Weinhold, NBO 6.0 : Natural bond orbital analysis program, J. Comput. Chem. 34 (2013) 1429–1437. doi:10.1002/jcc.23266.

[27] S.M.D. Rizvi, S. Shakil, M. Haneef, A simple click by click protocol to perform docking: AutoDock 4.2 made easy for non-bioinformaticians., EXCLI J. 12 (2013) 831–57. http://www.ncbi.nlm.nih.gov/pubmed/26648810.

[28] K.-C. Hsu, Y.-F. Chen, S.-R. Lin, J.-M. Yang, iGEMDOCK: a graphical environment of enhancing GEMDOCK using pharmacological interactions and post-screening analysis, BMC Bioinformatics. 12 (2011) S33. doi:10.1186/1471-2105-12-S1-S33.

[29] R. Dash, T. Bin Emran, M.N. Uddin, A. Islam, M. Junaid,Molecular docking of fisetin with AD associated AChE, ABAD and BACE1 proteins, Bioinformatics. 10 (2014) 562-568. doi: 10.6026/97320630010562.

[30] L. Carlsson, O. Spjuth, S. Adams, R.C. Glen, S. Boyer, Use of historic metabolic biotransformation data as a means of anticipating metabolic sites using MetaPrint2D and Bioclipse, BMC Bioinformatics. 11 (2010) 362. doi:10.1186/1471-2105-11-362.

[31] Teague, Davis, Leeson, Oprea, The Design of Leadlike Combinatorial Libraries., Angew. Chem. Int. Ed. Engl. 38 (1999) 3743–3748. http://www.ncbi.nlm.nih.gov/pubmed/10649345.

[32] M.T.H. Khan, Predictions of the ADMET properties of candidate drug molecules utilizing different QSAR/QSPR modelling approaches., Curr. Drug Metab. 11 (2010) 285–95. http://www.ncbi.nlm.nih.gov/pubmed/20450477.

[33] T. Sander, J. Freyss, M. von Korff, C. Rufener, DataWarrior: An Open-Source Program For Chemistry Aware Data Visualization And Analysis, J. Chem. Inf. Model. 55 (2015) 460–473. doi:10.1021/ci500588j.

[34] A. Husain, A. Ahmad, S.A. Khan, M. Asif, R. Bhutani, F.A. Al-Abbasi, Synthesis, molecular properties, toxicity and biological evaluation of some new substituted imidazolidine derivatives in search of potent anti-inflammatory agents, Saudi Pharm. J. 24 (2016) 104–114.

[35] I. Azad, M. Nasibullah, T. Khan, F. Hassan, Y. Akhter, Exploring the novel heterocyclic derivatives as lead molecules for design and development of potent anticancer agents, J. Mol. Graph. Model. 81 (2018) 211-228, https://doi.org/10.1016/j.jmgm.2018.02.013.

[36] S.R. Mahalle, P.D. Netankar, S.P. Bondge, R.A. Mane, An efficient method for Knoevenagel condensation: a facile synthesis of 5-arylidenyl 2,4-thiazolidinedione, Green Chem. Lett. Rev. 1 (2008) 103–106. doi:10.1080/17518250802139881.

[37] D. Arora, J. Dwivedi, S. Kumar, D. Kishore, Greener approach toward the generation of dimedone derivatives, Synth. Commun. 48 (2018) 115–134. doi:10.1080/00397911.2017.1387924.

[38] A. McCluskey, P.J. Robinson, T. Hill, J.L. Scott, J.K. Edwards, Green chemistry approaches to the Knoevenagel condensation: comparison of ethanol, water and solvent free (dry grind) approaches, Tetrahedron Lett. 43 (2002) 3117–3120. doi:10.1016/S0040-4039(02)00480-X.

[39] J. van Schijndel, L.A. Canalle, D. Molendijk, J. Meuldijk, The green Knoevenagel condensation: solvent-free condensation of benzaldehydes, Green Chem. Lett. Rev. 10 (2017) 404–411. doi:10.1080/17518253.2017.1391881.

[40] Y. Ren, C. Cai, Knoevenagel Condensation of Aromatic Aldehydes with Active Methylene Compounds using a Catalytic Amount of Iodine and K 2 CO 3 at Room Temperature, Synth. Commun. 37 (2007) 2209–2213. doi:10.1080/00397910701397375.

[41] J. Sanchez-Marquez, New advances in conceptual-DFT: an alternative way to calculate the Fukui function and dual descriptor, J. Mol. Model. 25 (2019) 1–7. doi:10.1007/s00894-019-4000-0.

[42] J. Sanchez-Marquez, D. Zorrilla, V. Garcia, M. Fernandez, Introducing a new bond reactivity index: Philicities for natural bond orbitals, J. Mol. Model. 24 (2018) 25. doi:10.1007/s00894-017-3553-z.

[43] M.H. Jamroz, Vibrational Energy Distribution Analysis (VEDA): Scopes and limitations, Spectrochim. Acta Part A Mol. Biomol. Spectrosc. 114 (2013) 220–230. doi:10.1016/j.saa.2013.05.096.

[44] M.P. Andersson, P. Uvdal, New scale factors for harmonic vibrational frequencies using the B3LYP density functional method with the triple-ζ basis Set 6-311+G(d,p), J. Phys. Chem. A. 109(2005) 2937-2941. doi:10.1021/jp045733a.

[45] I. Azad, A. Jafri, T. Khan, Y. Akhter, M. Arshad, F. Hassan, N. Ahmad, A. Rahman Khan, M. Nasibullah, Evaluation of pyrrole-2,3-dicarboxylate derivatives: Synthesis, DFT analysis, molecular docking, virtual screening and in vitro anti-hepatic cancer study, J. Mol. Struct. 1176 (2019) 314–334. doi:10.1016/j.molstruc.2018.08.049.

[46] Joseph M. Hornback, Organic Chemistry Second Edition, (2005).

[47] Donald L. Pavia, Gary M. Lampman, George S. Kriz, James A. Vyvyan, Introduction to Spectroscopy, (2008).

[48] I.A. Konstantinov, L.J. Broadbelt, Regression formulas for density functional theory calculated 1H and 13C NMR chemical shifts in toluene-d8, J. Phys. Chem. A. 115 (2011) 12364-12372. doi:10.1021/jp2060975.

[49] T.S. Renuga Devi, J. Sharmi Kumar, G.R. Ramkumaar, DFT analysis on the molecular structure, vibrational and electronic spectra of 2-(cyclohexylamino)ethanesulfonic acid, Spectrochim. Acta - Part A Mol. Biomol. Spectrosc. 137 (2015) 761-777. doi:10.1016/j.saa.2014.08.121.

[50] E. Khan, A. Shukla, A. Srivastava, Shweta, P. Tandon, Molecular structure, spectral analysis and hydrogen bonding analysis of ampicillin trihydrate: A combined DFT and AIM approach, New J. Chem. 39 (2015) 9800-9812. doi:10.1039/c5nj01779c.

[51] A.G. Al-Sehemi, A. Irfan, A.M. Asiri, Y.A. Ammar, Molecular design of new hydrazone dyes for dye-sensitized solar cells: Synthesis, characterization and DFT study, J. Mol. Struct. 1019 (2012) 130–134. doi:10.1016/j.molstruc.2012.02.035.

[52] R.K. Roy, S. Krishnamurti, P. Geerlings, S. Pal, Local Softness and Hardness Based Reactivity Descriptors for Predicting Intra - and Intermolecular Reactivity Sequences: Carbonyl Compounds. J. Phys. Chem. A 102 (1998) 3746-3755.

[53] P.K. Chattaraj, B. Maiti, U. Sarkar, Philicity: A unified treatment of chemical reactivity and selectivity, J. Phys. Chem. A. 107 (2003) 4973–4975. doi:10.1021/jp034707u.

[54] D. Santos-Martins, S. Forli, M.J. Ramos, A.J. Olson, AutoDock4(Zn): an improved AutoDock force field for small-molecule docking to zinc metalloproteins., J. Chem. Inf. Model. 54 (2014) 2371–9. doi:10.1021/ci500209e.

GRAPHICAL ABSTRACT